BENEMÉRITA UNIVERSIDAD AUTÓNOMA DE PUEBLA

INSTITUTO DE FÍSICA “LUIS RIVERA TERRAZAS”

“ADIABATIC GAUGE POTENTIAL APPROACH TO CHARACTERIZE THE ONSET OF CHAOS IN A MANY-BODY QUANTUM SYSTEM WITH LOCAL PERTURBATIONS”

TESIS

QUE PARA OBTENER EL GRADO DE

MAESTRO EN CIENCIAS (FÍSICA)

PRESENTA

JULIO CESAR TEXCA GARCIA

DIRECTORES DE TESIS

DR. EDUARDO JONATHAN TORRES HERRERA

No. de CVU: 1021517

NOVIEMBRE DE 2025

Universidad Autónoma de Puebla
Instituto de Física "Luis Rivera Terrazas"

Adiabatic gauge potential approach to characterize the onset of chaos in a many-body quantum system with local perturbations

Tesis presentada por

Lic. Julio Cesar Texca Garcia

para obtener el grado de

Maestro en Ciencias
(Física)

Dirigida por
Dr. Eduardo Jonathan Torres Herrera

Puebla, México
Noviembre 2025

Agradecimientos

Le agradezco a mi familia que han sido el pilar en toda mi vida y mi gran inspiración para superarme día a día, en especial a mis padres que me han formado como persona, por darme todo su apoyo y por las valiosas enseñanzas que me han dado. También agradezco a las personas que me han acompañado en esta larga travesía llamada vida, mis amigos (Alfredo, Michell, Alejandro, Edmundo y Aurora), que durante estos años han aportado tanto a mi vida, un sin fin de experiencias y enseñanzas. A Samantha por su amistad incondicional y sus valiosos consejos. Al Dr. Jonathan Torres por guiarme durante este trabajo. Al Insituto de Física por las excelentes personas con las que me he cruzado y por el conocimiento que he adquirido en mi corta estadía. Finalmente agradezco a la SECIHTI que financió mis estudios de maestría. Agradezco el apoyo financiero de la SECIHTI bajo el proyecto CF-2023-I-1748.

Dedicado a mis padres Esther Garcia y Marino Texca.

Adiabatic gauge potential approach to characterize the onset of chaos in a many-body quantum system with local perturbations

Resumen

En este trabajo estudiamos el llamado potencial adiabático de norma. Para nuestro trabajo empleamos dos modelos paradigmáticos de sistemas cuánticos de muchas partículas, el modelo de Heisenberg unidimensional de espín 1/2 con pertubaciones locales y el modelo de Aubry-André con interacciones. La primera parte de nuestro trabajo consiste en caracterizar el comportamiento de los modelos con herramientas convencionales de la teoría de matrices aleatorias. En particular, estudiamos las propiedades espectrales y la estructura y estadística de los estados propios de energía. Finalmente, estudiamos la transición del caos usando el potencial adiabático de norma. Se muestra que el potential adiabático de norma es más sensible para detectar la transición que diagnosticos tradicionales de la teoría de matrices aleatorias.

Adiabatic gauge potential approach to characterize the onset of chaos in a many-body quantum system with local perturbations

Abstract

In this work we study the so-called adiabatic gauge potential as a diagnostic of quantum many-body chaos. For our proposals we employ two paradigmatic models of many-body quantum systems, the one-dimensional Heisenberg spin-1/2 model with an on-site defect that can break integrability and, the interacting Aubry-André model. The first part of the work consists of characterizing the behavior of these models with conventional tools of random matrix theory. In particular, by studying the spectral properties and the structure and statistics of energy eigenstates. Finally, we study the transition to chaos in these models by means of the adiabatic gauge potential. We show that the adiabatic gauge potential is more sensitive to detect the transition than conventional diagnostics of random matrix theory.

Participation in events

- Adiabatic gauge potential approach to characterize the onset of chaos in a many-body quantum system with a quasiperiodical potential, Julio Cesar Texca Garcia, Eduardo Jonathan Torres Herrera, NQSTI International School: advances in solid-state quantum technologies, Catania, Italy (2025).

- Adiabatic gauge potential approach to characterize the onset of chaos in a many-body quantum system with a quasiperiodical potential, Julio Cesar Texca Garcia, Eduardo Jonathan Torres Herrera, Quantum Chaos 2025 - International Conference, Puebla, Mexico (2025).

- Adiabatic gauge potential as a tool to detect the onset of chaos in many-body quantum systems, Julio Cesar Texca Garcia, Eduardo Jonathan Torres Herrera, ICTP: Advanced School and Conference on Quantum Matter, Trieste, Italy (2025).

Content

Chapter 1

Introduction

The behavior of integrable and non-integrable classical Hamiltonian systems are now well understood. In contrast, chaos in quantum systems have been a puzzle for a long time, especially in recent times for interacting systems. Classical chaos is usually described in terms of an exponential sensitivity of trajectories in phase space to initial conditions. However, in the quantum realm, chaos cannot be described using physical trajectories because the Heisenberg uncertainty principle rules this out. The understanding of quantum chaos is very important in part because nowadays it is accepted as a fundamental ingredient for the application of statistical mechanics and thermodynamics [1, 2]. In the broad field of non-equilibrium many-body quantum physics, the behavior of isolated systems following a sudden disturbance has become an important topic of study.

Actually the study of quantum many-body systems is relevant in different areas of physics. With the emergence of quantum computing the study of many-body quantum systems is primordial for developing of this technology, chaotic effects in quantum computing have been studied, for instance [3, 4, 5]. Spin-1/2 models have been implemented on modern platforms, in [6] a many-body dynamical phase transition with a 53-qubit quantum simulator has been studied. In [7] many-body quantum systems with ultra cold gasses are studied. Finally, in [8] it was proposed a way to experimentally detect many-body quantum chaos. Alternatively, these systems have been used in Cosmology, for instance [9] has studied the implications of quantum chaos in Cosmology through the AdS-CFT correspondence.

In the past five decades, random matrix theory (RMT) has shown an exceptional success in the study of quantum chaos. Following the work of Wigner, who introduced random matrices to the realm of physics [10] and the subsequent classification of Dyson

in symmetry classes [11], Bohigas, Giannoni and Schmit [12] conjectured that energy level statistics of all quantum systems whose classical analog is chaotic should show level repulsion, just like eigenvalues of one of the three classical Gaussian ensembles of RTM, the orthogonal ensemble (GOE), the unitary ensemble (GUE) or the symplectic ensemble (GSE) [13]. The degree of level repulsion depends on the symmetries of the system. In addition, quantum systems whose classical counterparts are integrable, according to the Berry-Tabor conjecture [14], have uncorrelated energy levels, just like random variables in a Poisson process, so level repulsion is absent. There exist quantum systems that have no classical analog, like systems composed by spin-1/2 particles, electrons for instance. Despite of this fact, RMT-like energy level repulsion in this kind of systems has been considered as a signature of quantum chaos.

Traditional methods employing some standard tools have been applied to the study of the transition between integrable and chaotic behavior in quantum systems. These methods are mainly based in energy level statistics and structure of energy eigenstates. However, the involved tools are, in many cases, not enough sensitive to detect the onset of chaos when an integrability-breaking term is included in the system. Specifically, traditional diagnostics of quantum chaos can fail to detect precisely the onset of chaos when the strength of an integrability-breaking term is weak.

An alternative method to detect chaos in quantum systems was proposed in [15]. It was claimed and demonstrated that so-called adiabatic gauge potential (AGP) [16], which generates adiabatic deformations between eigenstates and encodes information on both level spacings and the matrix elements of local operators, is significantly more sensitive to detect the onset of quantum chaos compared to traditional methods. Another advantage of the AGP approach over other methods solely based on energy levels is that in order to reveal the chaotic nature of the system no desymmetrization or even unfolding are needed.

Mathematically, the distance between nearby neighbors, also called Fubini-Study metric [16, 17], can be expressed as a Frobenius norm of the AGP [16, 17]. In [16] it was claimed that the Frobenius norm should scale exponentially with the system size in chaotic systems. In this context, quantum chaos appears as an exponential sensitivity of eigenstates to tiny perturbations, serving as a counterpart to classical chaos. Later, in [15] it was explicitly found that the norm of the AGP scales exponentially with system size when the system is chaotic, whereas for integrable systems, it develops a polynomial scaling with system size. More recent studies have extended the study of the AGP to integrability

breaking terms like next-nearest-neighbors interactions [18] and systems of free fermions [19], providing additional details.

Our proposal is to study the transition from the integrable regime to the chaotic regime for the one-dimensional and anisotropic Heisenberg model of spin-1/2 particles, also known as XXZ model, with a perturbation at a single site located at the middle of the chain and the interacting Aubry-André model employing the AGP as a diagnostic to detect the onset of chaos. The XXZ model with a single defect at the middle of the chain has been used to show that, despite being local, a perturbation can induce global effects in interacting quantum systems [20] and also could be enough to bring the system to a chaotic regime [21]. This Thesis has the following structure; in chapter 2 we introduce quantum chaos and random matrix theory and the quantities that we will use along our study. In chapter 3 we introduce the main characteristics of 1/2-spin models and provide details of the two models used in this work, the XXZ model with local perturbations and the interacting Aubry-André model, including the corresponding description of the Hamiltonians. In chapter 4 we present the results obtained for the XXZ model with local perturbations. In chapter 5 we present the results obtained for the interacting Aubry-André model. In chapter 6 we provide the conclusions and perspectives of our work.

1.1 Objectives

To investigate the transition from an integrable to a chaotic regime in the one-dimensional Heisenberg spin-1/2 model under local perturbations and the interacting Aubry-André model, employing as diagnostic the so-called adiabatic gauge potential.

1.1.1 Specific objectives

- Implement in the one-dimensional Heisenberg spin-1/2 model under local perturbations and the interacting Aubry-André model numerically, using a suitable programming language.
- Characterize the transition to chaos in the one-dimensional Heisenberg spin-1/2 model under local perturbations and the in Aubry-André model studying the energy level statistics.
- Characterize the transition to chaos in the one-dimensional Heisenberg spin-1/2 model

under local perturbations and the interacting Aubry-André model analyzing the structure and statistics of energy eigestates.

- Characterize the transition to chaos in the one-dimensional Heisenberg spin-1/2 model under local perturbations and the interacting Aubry-André model using the adiabatic gauge potential.

- Compare the different diagnostics for the characterization of the transition to chaos in the one-dimensional Heisenberg spin-1/2 model under local perturbations and the interacting Aubry-André model.

Chapter 2

Quantum chaos and random matrix theory

Deterministic chaos in classical systems can arise from the nonlinear nature of their equations of motion, leading to extreme sensitivity to tiny variations in initial conditions. Today, classical chaos theory is well established and frequently used as a limiting case for comparison with its quantum counterpart, when such a limit can be meaningfully defined. In early days of the theory of quantum chaos, the studies were performed for quantum systems with well defined classical limits like two-dimensional billiards [22]. Nevertheless, nowadays the notion of quantum chaos is used in a much broader context, for example the notion of quantum chaos has been extended to quantum many-body systems without a classical limit, as well as models with some intrinsic randomness or disorder in their structure.

Many ideas for the treatment of systems with strongly chaotic properties came from **random matrix theory (RMT)**, following Wigner's work, who introduced random matrices to the realm of physics [10]. Wigner's original proposal was to employ random matrices to capture the statistical properties of complex nuclei and nuclear reactions. Early uses of RMT were confined to nuclear physics and had no direct connection to quantum chaos. Because the processes in compound nuclei involve highly intricate interactions that can only be treated statistically, random matrices offer an effective and powerful tool for describing them.

Dyson showed that quantum mechanics provides a natural framework for classify-

ing random matrix ensembles [11]. There are three generic ensembles of random matrices, defined in terms of the symmetry properties of a given Hamiltonian.
i) Time-reversal invariant systems with rotational symmetry. The elements of the Hamiltonian matrix are random numbers without zero entries and satisfy

$$H_{nm} = H_{mn} = H^*_{mn}. \tag{2.1}$$

Where H^*_{mn} is the conjugate of H_{mn}.

ii) Systems in which time-reversal invariance is violated. For such systems, the Hamiltonian matrices are Hermitian, the elements of the Hamiltonian matrix are random complex numbers and satisfy

$$H_{mn} = [H^\dagger]_{nm}. \tag{2.2}$$

Where $H^\dagger$ is the adjunct matrix of H

iii) Time-reversal invariant systems without rotational symmetry. The elements of the Hamiltonian matrix are random 2x2 quaternions.

Since we are interested in the eigenvalue correlations, it is necessary to diagonalize the matrix, $H = UxU^{-1}$. The diagonalizing matrix U is in the orthogonal group $O(n)$ for the systems belonging to case i), in the unitary group $U(n)$ for the systems belonging to case ii) and in the unitary symplectic group $USp(2n)$ for the systems belonging to the case iii) [23]. Accordingly, the three symmetry classes are referred to as orthogonal, unitary and symplectic. It is common to consider a Gaussian distribution as the probability densities for random entries H_{nm}. Therefore, the three symmetric classes together with the probability densities define the Gaussian ensembles of RMT: the Gaussian orthogonal ensemble (GOE), the Gaussian unitary ensemble (GUE) and the Gaussian symplectic ensemble (GSE).

Bohigas, Giannoni and Schmit [12] conjectured that energy level statistics of all quantum systems whose classical analog is chaotic should show level repulsion, just like eigenvalues of one of the three classical Gaussian ensembles of RTM, the orthogonal ensemble (GOE), the unitary ensemble (GUE) or the symplectic ensemble (GSE) [13]. In particular energy level statistics of time-reversal-invariant systems whose classical analogs are strongly chaotic systems then they show the same fluctuation properties as predicted by GOE. Quantum systems whose classical counterpart is integrable, according to the Berry-Tabor conjecture [14], have uncorrelated energy levels, just like random variables in a Poisson process, so level repulsion is absent. There exist quantum systems that have no classical

analog, like systems composed by spin-1/2 particles, electrons for instance. Despite of this fact, RMT-like energy level repulsion in this kind of systems has been considered as a signature of quantum chaos.

2.1 Energy level statistics

Level statistics is the most common approach to detect chaos. We decided to use three different indicators, each one in order to perform a better characterization of the systems. We use the mean ratio of energy-level spacings $\langle\tilde{r}\rangle$ to characterize the transition from an integrable regime to the chaotic regime, since it is an excellent tool for characterizing the transition to chaos in terms of a single number. Secondly, we studied the level spacing distribution $P(s)$, this is a standard tool to study level repulsion between consecutive energy eigenvalues. Finally, we studied the so-called level number variance (LNV), in contrast to mean ratio and level spacing distribution that can indicate short range correlations between of energy-level spacings, level number variance study long range correlations.

2.1.1 Ratio between spacings

To study the level spacing distribution one has to perform a procedure called unfolding. The unfolded spectrum has automatically a mean level spacing equal to one, and its statistics can thus directly be compared with those of RMT. There are many procedures to unfold the spectrum and they present difficulties, specially in many-body problems when the Hilbert space increase with the number of particles in the system, because they present a dependence on the mean level spacing δ [24]. We define the spacing between nearest neighbors as

$$s_n = \epsilon_{n+1} - \epsilon_n, \qquad n \in \{1, 2, 3, ..., N-1\}. \tag{2.3}$$

Where $\epsilon_n = E_n/\delta$. To avoid this difficulties Oganesyan and Huse [25] proposed to compute instead the ratios $\tilde{r}_n$ between consecutive level spacings, defined by

$$\tilde{r}_n = \frac{\min(s_n, s_{n-1})}{\max(s_n, s_{n-1})} = \min\left(r_n, \frac{1}{r_n}\right), \qquad n \in \{1, 2, 3, ..., N-2\}. \tag{2.4}$$

With

$$r_n = \frac{s_n}{s_{n-1}}. \tag{2.5}$$

This quantity has the advantage that it does not require unfolding since the ratios of consecutive level spacings are independent of the mean level spacing δ. This new quantity yields an analytic estimate for the mean value of $\langle\tilde{r}\rangle$, widely used in the literature as a measure of chaoticity. It has been found that $\langle\tilde{r}\rangle \approx 0.38629$ for integrable systems and $\langle\tilde{r}\rangle \approx 0.53590$ for chaotic systems with GOE-like statistics for its eigenvalues [26].

2.1.2 Level spacing distribution

However, despite of the mean ratio of energy-level spacings offers an analysis in terms of a singles number, it does not give us details about correlations presented in the spectrum. Therefore, we resort to the study of level spacing distribution and level number variance.

Remarkably, a strong universality emerges in the spectral correlations across a wide variety of systems, ranging from atoms and molecules to quantum-chaotic and disordered systems. The analysis of level statistics is the most common approach to detect chaos. To use level statistics, it is necessary to unfold part of the spectrum considered. The tails of spectrum in physical systems do not present chaotic behavior, so we focus in the central part, for each system size we exclude a certain percentage of the tails. The unfolding consist of stretching the spectrum to normalize the density of state to unity. This is done by fitting the staircase function, defined for the increasingly sorted eigenvalues $E_1, ..., E_N$ as

$$\eta(E) = \sum_{n=1}^{N} \Theta(E - E_n) \tag{2.6}$$

The unfolding corresponds to mapping the eigenvalues onto the smooth function obtained,

$$E_n \to \epsilon_n = \bar{\eta}(E_n). \tag{2.7}$$

The unfolding methods are divided into local and global methods. We decided to use a global unfolding since local unfolding does not preserve global correlations, these are needed to study long range correlations as level number variance. Following the work [27] we use a 7th order polynomial regression.

Consider the nearest neighbor spacing distribution $P(s)$. It is the probability density of finding two adjacent levels in the distance s. For chaotic systems, the level spacing distribution follows the Wigner-Dyson distribution, also known as the Wigner surmise,

$$P_{\mathrm{WD}}(s) = \frac{\pi}{2} s \exp\left(-\frac{\pi}{4} s^2\right). \tag{2.8}$$

Which indicates that the eigenvalues are highly correlated in the sense that they repel each other. If the distance is quite short $s \sim 0$ then we have the behavior

$$P_{\mathrm{WD}}(s) \sim s. \tag{2.9}$$

This means that close to 0 the levels present a linear repulsion. Finally, if we consider the limit $s \to 0$, the probability of finding two levels with the same energy decreases, in particular $P_{WD}(0) = 0$. This is a typical behavior in quantum chaotic systems.

For integrable models is typical that the energy levels are uncorrelated and the level spacing distribution is Poissonian,

$$P_{\mathrm{P}}(s) = \exp(-s). \tag{2.10}$$

In this case as $s \to 0$, the probability to find two levels with the same energy is 1. There are some exceptions that include a "picket-fence" kind of spectra [28] and systems with an excessive number of degeneracies [29]. This last point emphasizes the importance of removing some symmetries from the system.

2.1.3 Level number variance

To have access to long-range correlations one employs the level number variance $\Sigma^2(l)$. The level number variance provides a useful way to examine the characteristics of the energy spectrum across all correlation-length scales. In contrast to the nearest neighbor level spacing $P(s)$ which measures only short range correlations, the level number variance $\Sigma^2(l)$ probes the spectrum over all correlation lengths l. The level number variance describes the fluctuations of the number $N(l, g)$ of levels contained in a the interval $[g, g+l]$ of length l. The spectral rigidity, introduced by Dyson and Mehta [30, 23] is closely related to $\Sigma^2(l)$. It is defined as

$$\Sigma^2(l) \equiv \langle N(l,g)^2 \rangle - \langle N(l,g) \rangle^2, \tag{2.11}$$

where $N(l, g)$ gives the number of states in the interval $[g, g + l]$ on the unfolded scale and $\langle ... \rangle$ represents the average over different values of g. If the energy levels are completely uncorrelated, like integrable systems, or for Poisson distributions, the level number variance grows linearly

$$\Sigma^2(l) = l, \tag{2.12}$$

this means that the fluctuations are large, since there is not repulsions between levels. On the other hand for chaotic systems and matrices that belong to the GOE, the level number variance $\Sigma^2(l)$ behaves as

$$\Sigma^2(l) = \frac{2}{\pi^2}[ln(2\pi l) + \gamma + 1 - \frac{\pi^2}{8}]. \tag{2.13}$$

where $\gamma = 0.5772...$ is the Euler constant. Level repulsion leads to rather rigid spectra and fluctuations are less significant than in regular systems [20] due to long-range correlations.

2.2 Structure and statistics of eigenstates

RMT allows us to make an important statement about the eigenvectors of random matrices, the eigenvectors of random matrices are random unit vector because the components of eigenstates satisfy a Gaussian distribution, which are real in the case of matrices that belong to the GOE. The study of eigen states are quite important since it is a fundamental ingredient for the study of thermalization [31], or Anderson localization [32].

It is shown that when entering into chaotic behavior, the structure of eigenstates change remarkably [24]. It is usual to choose a basis according to physical reasons to describe the eigenstates structure, the mean-field basis is the most common chosen basis. Nevertheless, it is clear that there are bases in which the eigenstates are very well localized. Indeed, there is a special basis where all eigensates are completely localized. This could be a problem because the statical properties of the eigenstates are not invariant with respect the choice of the basis.

Commonly, a quantum many body system described by a Hamiltonian H can be separated in two parts as $H = H_0 + V$, where H_0 is an integrable Hamiltonian and V plays the role of perturbation. The mean-field basis is built by eigenstates of H_0. When the perturbation V is zero, the system is integrable and the eigenstates are localized. When the perturbation is applied, integrability can be disrupted. The original unperturbed basis states become mutually coupled and combine to form new eigenstates. However, because particle interactions are typically short-ranged, only neighboring unperturbed states are directly connected. These states form a subspace that corresponds to an energy shell [33]. For weak perturbations, only a few unperturbed basis states contribute to each new eigenstate, meaning the eigenstate remains localized. When the perturbation becomes large, more and more unperturbed states are coupled and new eigen-states can spread broadly in

subspace and fulfill the shell. When all basis states participate in the eigenstate structure, also known as ergodic case, the expansion coefficients of new eigenstates in the mean-field basis satisfy a Gaussian distribution and these eigenstates are called random eigenstates or chaotic eigenstates [34].

2.2.1 Inverse participation ratio

Given an eigenstate $|\psi_n\rangle = \sum_n C_m^n |m\rangle$, where $C_m^n = \langle m|\psi_n\rangle$. To analyze the structure of $|\psi_n\rangle$, we consider the inverse partition ratio (IPR) defined as

$$IPR_n = \sum_{m=1}^{N} |C_m^n|^4. \tag{2.14}$$

where N is the dimension of the local Hilbert space. The IPR measures how much the eigenstates are delocalized on the provided basis $\{|m\rangle\}$, that is, how many basis states participate in the structure of the state $|\psi_n\rangle$. IPR_n can take values in the range $[N^{-1}, 1]$. The lower bound corresponds to the case where $|\psi_n\rangle$ uniformly populates all basis states, namely, $|C_m^n|^2 = N^{-1}$. An eigenstate is chaotic if it samples most of the Hilbert space without any preference, which means $IPR_n \propto N^{-1}$. The upper bound corresponds to the case where $|\psi_n\rangle$ is completely localized on a single basis state [35]. For eigenstates that belong to matrices of GOE the IPR is [36]

$$IPR_{GOE} = \frac{3}{N+2}. \tag{2.15}$$

The IPR has been one of the main tools in assessing the localization properties of eigenstates of many-body quantum systems [37].

2.2.2 Porter-Thomas distribution

The Porter-Thomas distribution was born as a probability distribution used in nuclear physics, especially in the statical description of nuclear resonances widths [38]. For chaotic systems, the weights C_m^n follow the Porter-Thomas distribution

$$P_{PT}(|C_m^n|^2) = \left(\frac{N}{2\pi|C_m^n|^2}\right)^{1/2} \exp\left(-\frac{N}{2}|C_m^n|^2\right). \tag{2.16}$$

It is an additional tool to determine whether the states are chaotic or not. As states are localized, the components fluctuate more and deviate from the Porter-Thomas distribution [37]. However, because the contributions of $|C_m^n|$ are quite small, it is usual to analyze

the distribution of $ln|C_m^n|$. According to the continuous random variables transformation theorem, let X a continuous random variable with probability distribution $f_X(x)$. We assume that a function g is differentiable and strictly monotone. Then the probability distribution function of the transformed random variable Y is given by

$$f_Y(y) = f_X(g^{-1}(y)) \left| \frac{dg^{-1}(y)}{dy} \right| \tag{2.17}$$

where $Y = g(x) = ln(x)$ and $x = |C_m^n|^2$. Since the logarithmic function is differentiable and strictly monotone, and $g^{-1}(y) = e^y$, then evaluating the Eq. (2.17) we have

$$f_Y(y) = \left(\frac{N}{2\pi}\right)^{1/2} exp\left(\frac{y - Ne^y}{2}\right). \tag{2.18}$$

2.3 Adiabatic gauge potential approach to detect the onset of chaos

There are many tools to detect the chaotic behavior in quantum systems, however most of them are not sensitive enough to detect the onset of the chaotic behavior when an integrable braking term is considered. Recently an alternative approach has been proposed as a tool to detect chaos in quantum systems, the adiabatic gauge potential (AGP) [15]. The AGP is the generator of adiabatic deformations between quantum eigenstates. In a precise sense, the distance between two eigenstates is the Frobenius norm of the AGP [16]. It has been observed that the AGP displays different scaling behaviors for integrable and chaotic systems. The AGP is remarkably accurate in distinguishing the chaotic systems from the integrable ones, since it is sensitive to integrability-breaking perturbations that are exponentially small in the system size [18]. This by far exceeds the sensitivity of standard probes of chaos, such as level statistics or mean ratio between consecutive spacings.

2.3.1 Adiabatic gauge potential

Consider a Hamiltonian $H(\gamma) = H_0 + \gamma V$, where H_0 can be chaotic or integrable, depending on a parameter γ. This Hamiltonian has a set of eigenstates $|n(\gamma)\rangle$, satisfying time-independent Schrödinger equation:

$$H(\gamma)|\psi_n(\gamma)\rangle = E_n(\gamma)|\psi_n(\gamma)\rangle. \tag{2.19}$$

It is possible to define a unitary transform that rotates these eigenstates

$$|\psi_n(\gamma)\rangle = U(\gamma)|\psi_n(0)\rangle \tag{2.20}$$

this unitary transformation is well defined, up to the choice of the phases of the vectors. The generator of this transformation is called the adiabatic gauge potential, denoted as $\mathscr{A}_\gamma$. The formal definition according to [19] is

$$\mathscr{A}_\gamma = i[\partial_\gamma U(\gamma)]U^\dagger(\gamma), \qquad \mathscr{A}_\gamma|\psi_n(\gamma)\rangle = i\partial_\gamma|\psi_n(\gamma)\rangle. \tag{2.21}$$

The relative phases of the eigenvectors could be chosen as an arbitrary function of γ. A convenient choice is setting all diagonal elements equal to zero.

$$\langle\psi_n(\gamma)|\mathscr{A}_\gamma|\psi_n(\gamma)\rangle \equiv 0. \tag{2.22}$$

The adiabatic evolution of its eigenstates is generated by (in units where $\hbar = 1$)

$$\mathscr{A}_\gamma|\psi_n(\gamma)\rangle = i\partial_\gamma|\psi_n(\gamma)\rangle. \tag{2.23}$$

Using the Hellmann-Feynman theorem

$$\langle\psi_m|\partial_\gamma|\psi_n\rangle = \frac{\langle\psi_m|\partial_\gamma H|\psi_n\rangle}{E_m - E_n}, \tag{2.24}$$

the matrix elements of the AGP are given by

$$\langle\psi_m|\mathscr{A}_\gamma|\psi_n\rangle = \frac{i}{\omega_{mn}}\langle\psi_m|\partial_\gamma H|\psi_n\rangle \tag{2.25}$$

where $\omega_{mn} = E_m(\gamma) - E_n(\gamma)$, $\partial_\gamma H$ is the operator conjugate to the coupling γ, and we make the dependence on γ implicit. Is needed to define the L_2 (Frobenius) norm, also called the Hilbert-Schmidt norm as

$$||\mathscr{A}_\gamma||^2 = \frac{1}{N}\sum_n \sum_{m\neq n} |\langle\psi_n|\mathscr{A}_\gamma|\psi_m\rangle|^2 \tag{2.26}$$

where N is the dimension of the Hilbert space. The previous expression is not practical because the norm of the exact AGP can be dominated by the smallest energy gaps between eigenstates, making it highly unstable and challenging to analyze. To resolve this issue, it is convenient to define a "regularized" AGP as

$$\langle\psi_m|\mathscr{A}_\gamma|\psi_n\rangle = -i\frac{\omega_{mn}}{\omega_{mn}^2 + \mu^2}\langle\psi_m|\partial_\gamma H|\psi_n\rangle \tag{2.27}$$

where μ is the small energy cutoff. With this change we now only consider transitions between energy shells of width μ. In the work [15] it was demonstrated that the most convenient choose of μ is $\mu \sim LN^{-1}$ with L being the system size. The norm of the regularized AGP reads

$$||\mathscr{A}_\gamma||^2 = \frac{1}{N}\sum_n \sum_{m\neq n} \frac{\omega_{mn}^2}{(\omega_{mn}^2+\mu^2)^2}|\langle\psi_n|\partial_\gamma H|\psi_m\rangle|^2 \tag{2.28}$$

$$= \int_{-\infty}^{\infty} d\omega \frac{\omega^2}{(\omega^2+\mu^2)^2}\overline{|f_\gamma(\omega)|^2} \tag{2.29}$$

where in the second equation we replace the summation with an integration over the energy difference $\omega_{mn} = E_m(\gamma) - E_n(\gamma)$ and

$$\overline{|f_\gamma(\omega)|^2} = \frac{1}{N}\sum_n \sum_{m\neq n} |\langle\psi_n|\partial_\gamma H|\psi_m\rangle|^2 \delta(\omega_{nm}-\omega) \tag{2.30}$$

Formally this function represents an average over eigenstates $|\psi_n\rangle$ of the sum of the squares of the off-diagonal matrix elements $|\langle\psi_n|\partial_\lambda H|\psi_m\rangle|^2$ with a fixed energy difference $\omega_{mn} = \omega$. Alternatively, we can rewrite the regularized AGP as a time integral [15, 19]

$$\mathscr{A}_\gamma = -\frac{1}{2}\int_{-\infty}^{\infty} dt\ \mathrm{sgn}(t) e^{-\mu|t|}(\partial_\gamma H)(t), \tag{2.31}$$

where $\mathrm{sgn}(t)$ is the sign function and

$$(\partial_\gamma H)(t) = e^{iHt}(\partial_\gamma H)e^{-iHt} \tag{2.32}$$

is the operator conjugate to the coupling λ in the Heisenberg representation.

If H_0 is chaotic, or if is integrable but the perturbation breaks integrability, then the norm of the AGP exhibits exponential scaling with the number of particles L.

$$\frac{||\mathscr{A}_\gamma||^2}{L} \sim e^{\kappa L} \tag{2.33}$$

for any finite parameter γ. This scaling should hold in the limit $L \to \infty$. On the other hand, if H_0 and also $H(\lambda)$ are integrable, then a polynomial bound of the AGP was found

$$\frac{||\mathscr{A}_\gamma||^2}{L} \sim L^p, \qquad p \in \mathbb{R}. \tag{2.34}$$

Chapter 3

Spin-1/2 models

Spin-1/2 models are widely used in physics to describe a extend number of phenomenons. In condensed matter physics these models are used to describe wide range of phenomena in materials. Spin-1/2 models can also be applied to other systems with two-level quantum degrees of freedom. In quantum Many-body systems these models provide a framework for understanding how a large number of interacting quantum particles behave, it is of main interest the study of many-body localization or thermalization for isolated systems. Finally, these models are used in quantum information since they are fundamental building blocks for quantum computers. These systems have been implemented experimentally, studied with nuclear magnetic resonance, optical lattice, trapped ions, superconducting circuits.

One of the most important models is the Heisenberg model developed by Werner Heisenberg also known as the XXZ model, this model was developed to study critical points and phase transitions of magnetic fields. This model is a relatively simple model, but it is still rich enough to exhibit interesting quantum phenomena such as phase transitions and entanglement. The XXZ model describes a system of L spin-1/2 particles, each one located at each site of a one-dimensional lattice. The particles can interact in pairs with nearest neighbors. The Hamiltonian of this system is given by

$$H_{\mathrm{XXZ}} = J \sum_{k=1}^{L-1} (S_k^x S_{k+1}^x + S_k^y S_{k+1}^y + \Delta S_k^z S_{k+1}^z), \tag{3.1}$$

$S_k^{x,y,z} = \sigma_k^{x,y,z}/2$ are the spin operators acting on the spin located at site k, and $\sigma^{x,y,z}$ are the Pauli matrices; we use units where $\hbar = 1$, J the coupling constant that sets the energy scale, and Δ is the anisotropy parameter. In this work we will use $J = 1$ and $\Delta = 0.48$,

this last value is motivated only to avoid total spin conservation, $\mathcal{S}^2 = (\sum_{k=1}^{L} \vec{S}_k)^2$, which happens when $\Delta = 1$ [39]. It is easy to show that this Hamiltonian is invariant under time reflection, namely the Hamiltonian (3.1) satisfies

$$H_{\mathrm{XXZ}} = \Theta H_{\mathrm{XXZ}} \Theta^{-1}, \tag{3.2}$$

where Θ is the time reversal operator.

The terms with $S_k^{x,y}$ and $S_{k+1}^{x,y}$ in Eq. (3.1) represent couplings between two adjacent sites, meanwhile the summation with $S_k^z S_{k+1}^z$ are Ising-like interactions between two spins [40]. Open boundary conditions are considered in order to avoid translational symmetry.

In the context of condensed matter, when $J < 0$, the energy is minimized when the spins are parallel to each other and we have the ferromagnetic version of the model. For $J > 0$, anti-parallel orientation is instead favored and we have an antiferromagnetic model [41]. Hamiltonian (3.1) represents an integrable model, first in the sense that it is possible to solve it exactly by the Bethe Ansatz [42] and second because it does not show energy level repulsion.

To describe a single spin-1/2 particle, it is needed to use the Hermitian operators $S^{x,y,z}$, then these operators are described according to $S_k^{x,y,z} = \sigma_k^{x,y,z}/2$, with $\sigma_k^{x,y,z}$ being the Pauli matrices, where

$$\sigma^x = \begin{pmatrix} 0 & 1 \\ 1 & 0 \end{pmatrix} \quad \sigma^y = \begin{pmatrix} 0 & -i \\ i & 0 \end{pmatrix} \quad \sigma^z = \begin{pmatrix} 1 & 0 \\ 0 & -1 \end{pmatrix}. \tag{3.3}$$

The quantum states of a single particle are described in terms of the operator S^z eigenstates, the spin up $|\uparrow\rangle = \begin{pmatrix} 1 \\ 0 \end{pmatrix}$ and the spin down $|\downarrow\rangle = \begin{pmatrix} 0 \\ 1 \end{pmatrix}$. The operators $S_k^{x,y,z}$ acting on the states according to

$$S^z|\uparrow\rangle = \frac{1}{2}|\uparrow\rangle, \qquad S^z|\downarrow\rangle = -\frac{1}{2}|\downarrow\rangle. \tag{3.4}$$

$$S^y|\uparrow\rangle = \frac{i}{2}|\downarrow\rangle, \qquad S^y|\downarrow\rangle = -\frac{i}{2}|\uparrow\rangle. \tag{3.5}$$

$$S^x|\uparrow\rangle = \frac{1}{2}|\downarrow\rangle, \qquad S^x|\downarrow\rangle = -\frac{1}{2}|\uparrow\rangle. \tag{3.6}$$

We use the S^z eigen states to represent the system states, this means that we represent the many particle states as tensor products of single-particle states.

Since each particle has an associated Hilbert space $\mathscr{C}^2$ of dimension 2, the many-body Hilbert space $\mathscr{H}$ for the entire system of L particles is the tensor product of all

individual Hilbert spaces,

$$\mathscr{H} = \mathscr{C}^2 \otimes ... \otimes \mathscr{C}^2. \tag{3.7}$$

Then the dimension of the many-body Hilbert space is $\mathscr{N} = 2^L$. However, we can exploit the fact that the Hamiltonian (3.1) is invariant under rotations around the z-direction. In this case, the total magnetization in z-direction, $\mathcal{S}^z = \sum_{k=1}^{L} S_k^z$, is conserved

$$[\mathcal{S}^z, H_{XXZ}] = 0. \tag{3.8}$$

Since the total spin magnetization on the z-direction is conserved the total Hilbert space is then separated in $L+1$ independent subspaces.

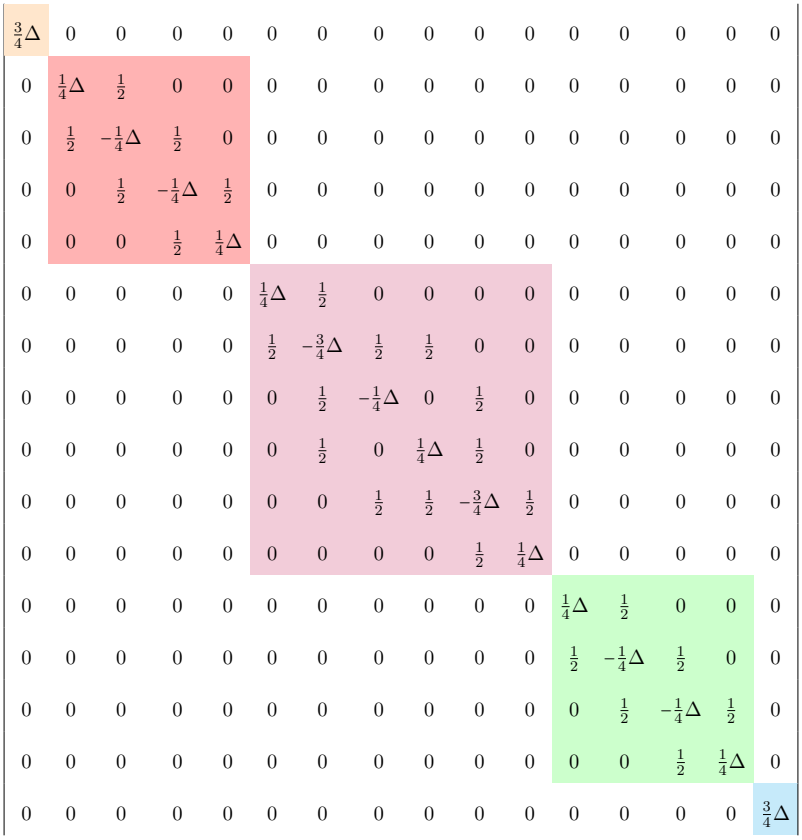

Figure 3.1: Matrix representation of the Hamiltonian (3.1) for $L = 4$ spins.

Figure 3.1 shows the matrix representation of the Hamiltonian (3.1) for $L = 4$ spins using as base the eigenstates of the S^z operator, the matrix is divided in $L + 1 = 5$ subspaces, each subspace has a different color. The orange block is the sector with $\mathcal{S}^z = -2$, the red block corresponds to the sector with $\mathcal{S}^z = -1$, the purple block corresponds to the

sector with $\mathcal{S}^z = 0$, the green block corresponds to the sector with $\mathcal{S}^z = 1$ and the cyan block corresponds to the sector with $\mathcal{S}^z = 2$. Another important fact is that this matrix is a sparse matrix, which means that there are a lot of zero entries out of the main diagonal, in Sec. 3.3 are given more details. The dimension of each subspace is given by

$$N = \frac{L!}{(L/2 + S^z)!(L/2 - S^z)!}. \tag{3.9}$$

Since we are interested in some statistical properties of energy eigenvalues and eigenstates, we choose to work in the subspace with $\mathcal{S}^z = 0$, which has the larger dimension $N = L!/(L/2)!^2$, this subspace is commonly known as the "half-filling sector". In the reminder of the work we will refer to this subspace as the half-filling sector, this will let us to reach larger system sizes in comparison with the full Hilbert space. For example, considering a system with $L = 18$ particles, the full Hilbert space has dimension $\mathcal{N} = 262,144$, while the dimension for the subspace with $\mathcal{S}^z = 0$ is $N = 48,620$. This is much better appreciated when dealing with numerical computations on a classical computer with finite memory.

3.1 Heisenberg model with a local perturbation

In the broad field of non-equilibrium quantum physics, the unitary evolution of an isolated system after an instantaneous perturbation has become a prominent subject [43]. The Heisenberg model under local perturbation is obtained by applying a magnetic field in the z-direction over a single site. The experiment [44] analyzes the quantum dynamics of an excitation created by flipping a single spin in the middle of a Heisenberg chain. The corresponding Hamiltonian is

$$H_{[L/2]} = H_{\mathrm{XXZ}} + \epsilon_1 S_1^z + \lambda S_{[L/2]}^z + \epsilon_L S_L^z. \tag{3.10}$$

Where $S_{[L/2]}^z$ is the magnetic field in the middle of the chain and λ its amplitude. It is important to note that when the chain is made up of an odd number of particles, $L/2$ is not an integer number, then we take the integer part of $L/2$. Additional impurities at the edges of the chain with corresponding amplitudes $\epsilon_{1,L}$ are introduced without compromising the integrability of the model, but to avoid parity and spin reversal symmetries. Separation in symmetry sectors or avoiding symmetries (disymmetrization) is important because mixing eigenvalues from different symmetry sectors which are independent when doing statistics could hide the chaotic nature of the system. The inclusion of the three different defects

does not prevent conservation of $\mathcal{S}^z$, then

$$[\mathcal{S}^z, H_{[L/2]}] = 0, \tag{3.11}$$

even after including the defects, we can still work in the subspace with total magnetization $\mathcal{S}^z = 0$.

In particular, when the site is the one at the middle of the chain, the induced defect can break the integrability of the XXZ model [45, 21]. This model has been studied in [21], according to this work the model presents a transition from an integrable to a chaotic regime in the interval [0,0.1] of the perturbation amplitude.

3.2 Aubry-André model

The Aubry-André Model describes interacting 1/2-spin particles, where each particle is located at each site of a one-dimensional lattice. The particles are coupled between their nearest neighbors and subject to an on-site potential in the z-direction. This model is used to study localization phenomena in one-dimensional quasiperiodic systems. We consider a quasiperiodic potential applied to every particle. The Hamiltonian that describes this system is given by

$$H_{AA} = H_{\mathrm{XXZ}} + \sum_{k=1}^{L} \lambda_k S_k^z. \tag{3.12}$$

Where $\lambda_k = \lambda\cos(2\pi k\beta + \phi)$ is known as the Harper potential [46], with λ being the strength of this potential. β an irrational number [47] which for tradition we use the inverse of the golden mean, $\beta = (\sqrt{5}-1)/2$. The phase ϕ is arbitrary and can be set to zero. The model given by Eq. (3.12) is known as the Aubry-André model [48], here with two-body interactions. The Harper potential does not prevent conservation of $\mathcal{S}^z$, then

$$[\mathcal{S}^z, H_{AA}] = 0, \tag{3.13}$$

so we can still work in the subspace with total magnetization $\mathcal{S}^z = 0$.

This model has been implemented in different modern platforms, in [49] the Aubry.André model has been implemented in superconducting circuits, in this work they experimentally showed that the system presents three different phases, the extend phase, the intermediate phase and the localized phase. According to the study done in [50] the system is in a chaotic regime when $\lambda \lesssim 0.7$, in an intermediate regime with extended but

non-ergodic states when $0.7 \lesssim \lambda \lesssim 1.7$, whereas it is in a localized regime for $\lambda \gtrsim 1.7$. This model has been implemented in optical lattices [51].

3.3 Numerical implementation of the models

Since our study will be numerical, we need to write the matrix representation of Hamiltonians (3.10) and (3.12). A suitable basis is the one formed by the eigenstates of S^z, that is, many-body states with alternating spins pointing up and down, also called product states. For instance, when $L = 4$ and at half-filling ($\mathcal{S}^z = 0$) the states are

$$\begin{aligned}
|\uparrow\rangle \otimes |\downarrow\rangle \otimes |\uparrow\rangle \otimes |\downarrow\rangle &\equiv |\uparrow\downarrow\uparrow\downarrow\rangle, \\
|\uparrow\rangle \otimes |\uparrow\rangle \otimes |\downarrow\rangle \otimes |\downarrow\rangle &\equiv |\uparrow\uparrow\downarrow\downarrow\rangle, \\
|\uparrow\rangle \otimes |\downarrow\rangle \otimes |\downarrow\rangle \otimes |\uparrow\rangle &\equiv |\uparrow\downarrow\downarrow\uparrow\rangle, \\
|\downarrow\rangle \otimes |\uparrow\rangle \otimes |\uparrow\rangle \otimes |\downarrow\rangle &\equiv |\downarrow\uparrow\uparrow\downarrow\rangle, \\
|\downarrow\rangle \otimes |\downarrow\rangle \otimes |\uparrow\rangle \otimes |\uparrow\rangle &\equiv |\downarrow\downarrow\uparrow\uparrow\rangle, \\
|\downarrow\rangle \otimes |\uparrow\rangle \otimes |\downarrow\rangle \otimes |\uparrow\rangle &\equiv |\downarrow\uparrow\downarrow\uparrow\rangle.
\end{aligned} \tag{3.14}$$

Once established the basis, one can determine how the terms in Hamiltonian (3.10) or (3.12) operate over the basis states. The terms inside the first summation of Eq. (3.1) is known as the *flip-flop* because it changes the orientation of adjacent spins as

$$\left(S_k^x S_{k+1}^x + S_k^y S_{k+1}^y\right) |\ldots\uparrow_k\downarrow_{k+1}\ldots\rangle = \frac{1}{2}|\ldots\downarrow_k\uparrow_{k+1}\ldots\rangle. \tag{3.15}$$

It only couples states with antiparallel adjacent spins. These terms leads to the off-diagonal elements of the Hamiltonian matrix. The term corresponding to the Ising interaction operates according to

$$\begin{aligned}
S_k^z S_{k+1}^z |\ldots\uparrow_k\uparrow_{k+1}\ldots\rangle &= \frac{1}{4}|\ldots\uparrow_k\uparrow_{k+1}\ldots\rangle. \\
S_k^z S_{k+1}^z |\ldots\uparrow_k\downarrow_{k+1}\ldots\rangle &= -\frac{1}{4}|\ldots\uparrow_k\downarrow_{k+1}\ldots\rangle.
\end{aligned} \tag{3.16}$$

This contributes to the main diagonal of the Hamiltonian matrix. We emphasize that due to the conservation of magnetization in z-direction, the Hamiltonian matrix has a block structure ($L + 1$ blocks) each one corresponding to a fixed value of $\mathcal{S}^z$. The Hamiltonian matrix will be implemented in a convenient computational language.

We will study statistical properties of energy eigenvalues and eigenstates, then the next technical step is to obtain those eigenvalues and eigenstates. That is, to solve the time-independent version of the Schrödinger equation

$$H|\psi_n\rangle = E_n|\psi_n\rangle. \tag{3.17}$$

Where $\{|\psi_n\rangle\}$ are eigenstates of H and $\{E_n\}$ are its eigenenergies. For this we will apply the numerical technique of exact diagonalization [52, 53, 54], which lets us to obtain the full set of eigenvalues and eigenstates of the Hamiltonian matrix corresponding to Eq. (3.10) and Eq. (3.12). We decided to implement these Hamiltonians in C++, because it is faster than other programming languages like Python or Mathematica. To diagonalize the Hamiltonian matrices we used the library Sparse from Eigen, since this library has been designed to work with sparse matrices like the matrices generated by the Hamiltonian Eq. (3.10) or Eq. (3.12). The algorithms were built from scratch and are available if needed.

The next step after model diagonalization is to use standard tools of random matrix theory to characterize the transition to chaos. For this aim, we study the energy spectrum and the statistics and structure of eigenstates. To characterize the energy spectrum we are going to use three indicators of chaos, level spacing distribution, the rigidity of the spectrum through the study of level number variance and the mean ratio between consecutive energy levels. First, we study short-range correlations through the ratio between consecutive energies to have a global perspective of the behavior with respect to the parameter λ in Eq. (3.10) and Eq. (3.12), then we study correlations between energy levels by means of the level spacing distribution. After that we study long-range correlations through the level number variance. To analyze the energy eigenstates we will use two quantities, the inverse participation ratio which distinguishes between localized states and extended states, usually related with integrability and chaos respectively, and the distribution of the energy eigenstates components, that for chaotic systems follow the so-called Porter-Thomas distribution.

Chapter 4

The XXZ model with local perturbations

The Hamiltonian implemented is given by Eq. (3.10)

$$H_{[1/2]} = \sum_{k=1}^{L-1} (S_k^x S_{k+1}^x + S_k^y S_{k+1}^y + \Delta S_k^z S_{k+1}^z) + \epsilon_1 S_1^z + \lambda S_{L/2}^z + \epsilon_L S_L^z. \tag{4.1}$$

Where we choose to work with number of particles $L = 8, 10, 12, 14, 16$, we also refer to L as the system size. As a remainder we take the anisotropy value $\Delta = 0.48$. For each system size we vary the perturbation amplitude λ in the interval $[0, 1.0]$ using steps of 0.5, we do this to characterize the transition from the integrable regime to the chaotic regime. We choose four amplitudes to implement standard methods to detect chaos, the chosen amplitudes are $\lambda = 0.0$, 0.3, 0.6 and 1.0. Once we diagonalize the Hamiltonian matrix, we obtain the eigenenergies for each number of particles and perturbation amplitude λ.

As we know, perturbations at the edges of the chain do not break the integrability of the system [55] and we include them just to avoid translational symmetry. Since our study is numeric, it is important to have a large sample space. However, this is not possible for the smallest system sizes L. Therefore, we take advantage of the impurities at the edges to make an ensemble and extend the sample space for the smallest system sizes. We fix the value of the defect at the beginning of the chain $\epsilon_1 = 0.1$ and the value of the defect at the end of the chain takes random values in the range $[-0.1, 0.1]$. The ensemble size for the systems L =8, 10 and 12 is 1000, and for the largest system sizes L = 14 and 16 the ensemble is 10, the reason is that the Hamiltonian matrix representations are matrices

of more than 1000x1000 entries; therefore, the time required to diagonalize is enormous, for the systems L = 16 it takes more than four days just to diagonalize one matrix. To have the average for the different spectral properties, first we calculated the property for each realization, and then we averaged for the entire ensemble. For instance, to calculate the level spacing distribution we fix the bins of the histogram and then we averaged the histogram for all realizations. For the ratios between consecutive spacings, we calculated them for each realization and then averaged them for the entire ensemble.

Figure 4.1 shows the eigenenergies obtained for four different perturbation amplitudes, we only graph eigenenergies for one realization of the ensemble. The figure is divided into five panels, each one corresponds to a different system size. Into the panels, the blue circles correspond to the perturbation amplitude λ = 0.0, the orange stars correspond to λ = 0.3, the green triangles correspond to λ = 0.6 and the red circles correspond to λ = 1.0. Panel (a) corresponds to the system size L = 8, in this graph is clear that the density of eigenenergies is not enough to carry out a statistical analysis due to the low density of eigenenergies. Panels (b), (c), (d), and (f) correspond to the system sizes L = 10, 12, 14, and 16 respectively.

In these graphs are depicted why it is important to perform ensembles, in particular for the smallest systems is clear that the density of energies is not enough to carry out a statistical study. Another important fact is that as we increase the system size the density of spectrum increase and therefore the sample space increase too, so it is not necessary to have a large ensemble for these systems, for instance an ensemble of 10 for the system size L = 16 gives us more than 100,000 eigen energies and one ensemble of 1000 for the system L = 8 gives us more than 50,000 eigen energies then the sample space in both cases is large enough to carry out the statistical study.

Based on the information in the figure 4.1 is not possible to deduce anything about the behavior of the systems since there are no differences of the spectrum, at least in the graphs, for different perturbation amplitudes λ. The panel (e) shows the spectrum for the systems L = 16, practically there are no differences between the spectrum, we cannot say whether a system is chaotic or not. Hence, it is important to unfold the spectrum and use methods such as the level spacing distribution or the level number variance to reveal the chaotic nature of the systems. We just consider the eigenvalues between the blue dashed lines since the eigenvalues outside the dashed lines are not correlated. We discard 20% of the total spectrum, discarding 10% at each site.

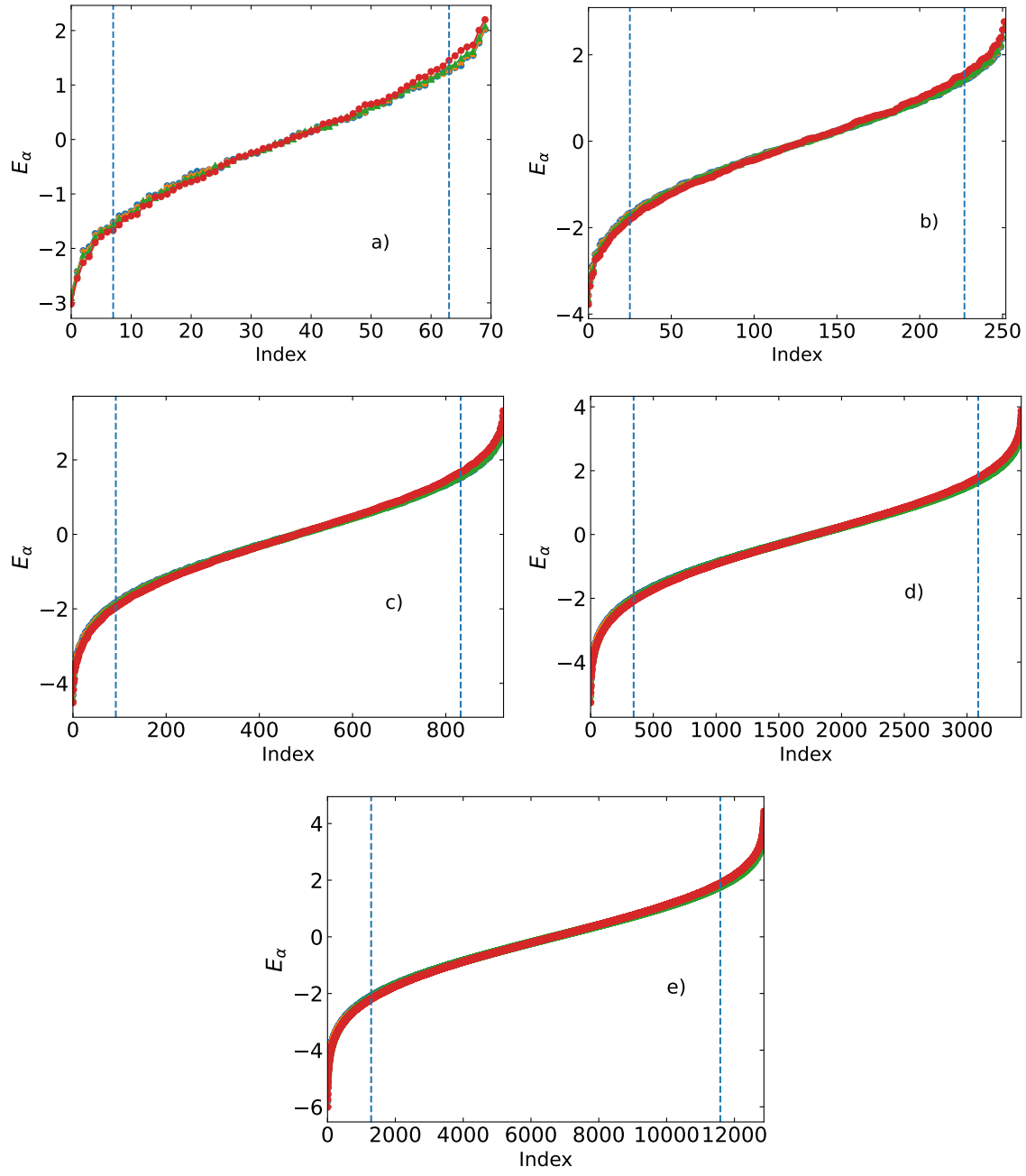

Figure 4.1: Plot of eigenenergies for different system sizes, a) $L = 8$, b) $L = 10$, c) $L = 12$, d) $L = 14$ and e) $L = 16$. In each graph is plotted four different energy spectrum belonging to four values of λ. The blue circles correspond to $\lambda = 0.0$, the orange stars correspond to $\lambda = 0.3$, the green triangles correspond to $\lambda = 0.6$ and the red circles correspond to $\lambda = 1.0$. The eigenenergies between the blue dashed lines represent the part of the spectrum we considered for our study.

4.1 Mean ratio between consecutive spacings

In this section, we present the results obtained for the mean ratio between consecutive spacings $\langle \tilde{r} \rangle$ for the XXZ model with local perturbations given by Eq. (4.6.3). The mean ratio between consecutive spacings is an excellent tool to study the transition in these systems since this quantity does not require unfolding, so we just calculate Eq. (2.4).

In figure 4.2 we show $\langle \tilde{r} \rangle$ for the different system sizes as a function of the perturbation amplitude λ. The figure is divided into five panels, each one corresponds to a different system size. The horizontal lines correspond to the theoretical predictions for chaotic (blue line) and integrable (red line) with $\langle \tilde{r} \rangle \approx 0.53590$ and $\langle \tilde{r} \rangle \approx 0.38629$ respectively.

Panel (a) shows the behavior of the smallest system size $L = 8$, the system for this size exhibits a different behavior than the others, there is a smooth transition from the integrable regime to the chaotic regime; however, it does not reach the chaotic regime and the $\langle \tilde{r} \rangle$ fluctuates around an intermediate zone. We attribute this kind of behavior to system effects, based on the information of this graph, it is not clear whether the system is chaotic or integrable. Panel (b) shows result for of the system size $L = 10$, here the behavior is clearer than the behavior displayed for the systems size $L = 8$, the system starts in the integrable regime, then as the perturbation amplitude increases the system transitions to the chaotic regime; however, there are fluctuations and it is not yet clear whether the system is in the chaotic regime or in an intermediate phase for the largest perturbation amplitudes. Panel (c) shows the behavior for the system size $L = 12$, in this graph the transition from the integrable regime to the chaotic regime is softer, the system stays in the chaotic regime after approximately $\lambda \approx 0.4$, in this zone the $\langle \tilde{r} \rangle$ fluctuates around the prediction for chaotic systems. Panel (d) shows the behavior for the system size $L = 14$, the transition for this system is faster than the transition shown in panel (c), the system reaches the chaotic regime approximately after $\lambda \approx 0.25$; for this system size the fluctuations are less than the fluctuations shown in panels (b) and (c). Finally, panel (e) shows the behavior for the system size $L = 16$, the transition is faster than all the other system sizes, the system reaches the chaotic regime approximately after $\lambda \approx 0.2$, and then the system stays in the chaotic regime for the largest amplitudes. However, according to the study carried out in [21] the system has another transition, but now from the chaotic regime to the integrable regime for perturbation amplitudes larger than 1, then our results are consistent with those reported in the literature.

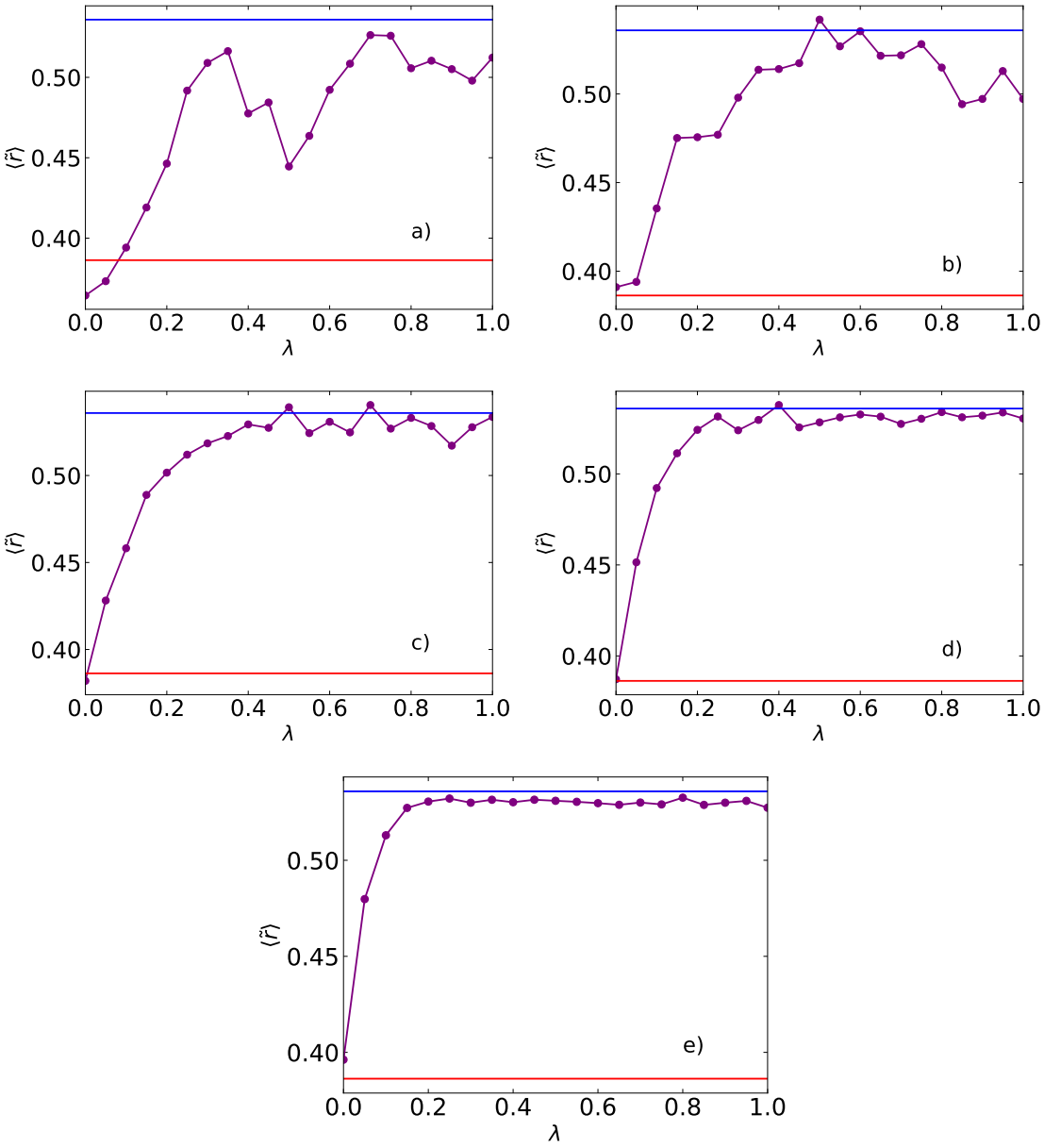

Figure 4.2: Mean ratio between consecutive spacings $\langle \tilde{r} \rangle$ for the XXZ model with local perturbations as function of the perturbation amplitude λ for different system sizes. The blue line corresponds to the prediction for chaotic systems $\langle \tilde{r} \rangle \approx 0.53590$ and the red line corresponds for integrable systems $\langle \tilde{r} \rangle \approx 0.38629$. The system sizes are a) $L = 8$, b) $L = 10$, c) $L = 12$, d) $L = 14$ and e) $L = 16$.

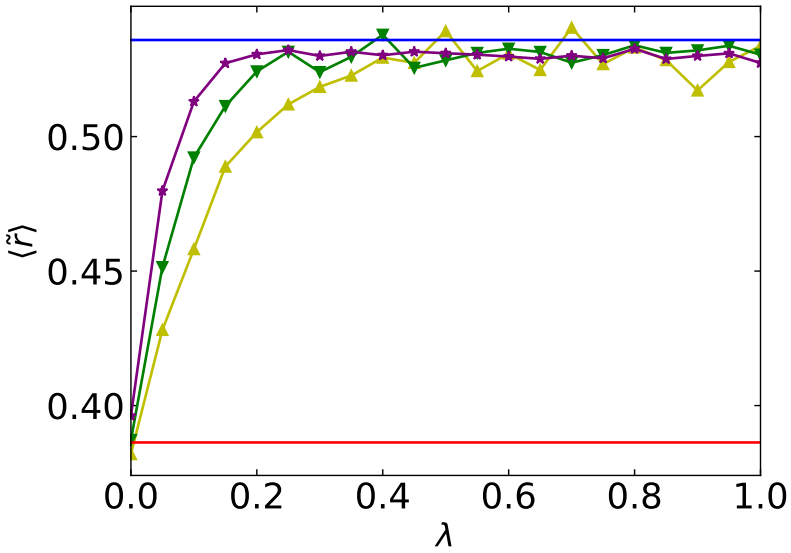

Figure 4.3: Mean ratio between consecutive spacings $\langle \tilde{r} \rangle$ for the XXZ model with local perturbations in function of the perturbation amplitude λ for three different systems sizes $L = 12$, 14 and 16. The yellow triangles are for $L = 12$, the green triangles are for $L = 14$ and the purple stars are for $L = 16$. The horizontal lines correspond to the theoretical predictions for chaotic (blue line) and integrable (red line) with $\langle \tilde{r} \rangle \approx 0.53590$ and $\langle \tilde{r} \rangle \approx 0.38629$ respectively.

In order to expose the dependence of the mean ratio $\langle \tilde{r} \rangle$ on the system size in Fig. 4.3 we graph $\langle \tilde{r} \rangle$ versus λ for the systems $L = 12$, 14 and 16. The blue line corresponds to the prediction for chaotic systems $\langle \tilde{r} \rangle \approx 0.53590$ and the red line corresponds for integrable systems $\langle \tilde{r} \rangle \approx 0.38629$. The yellow triangles correspond to the system size $L = 12$, the green triangles correspond to the system size $L = 14$ and the purple stars correspond to the systems size $L = 16$. In this figure we can see how the transition depends on the system size, the transition is faster as the system size increase, this is in agreement with the literature. Based on our results, we expect that for sufficiently large systems only an infinitesimal perturbation amplitude will be needed to break the integrability of the system.

In this graph it is clearer that in general $\langle \tilde{r} \rangle$ does not reach the value predicted by the GOE, we can explain it by arguing that we are studying a physical system instead of studying a GOE matrix; however, the values are close to these predictions.

4.2 Level spacing distribution

In this section, we study the level spacing distribution for the XXZ model with local perturbations, Eq.(4.6.3). This analysis is complementary to $\langle \tilde{r} \rangle$ since through level spacing distribution we study repulsion between eigenenergies. We use a global unfolding, since we will also study long-range correlations. We decided to perform a polynomial fitting of 7th order, can be found in Sec. 2 a general explanation of the procedure, although a more detailed description could be consulted in the reference [27]. Since our study is statistic, we report only the results obtained for the largest system size $L = 16$. We choose four different perturbation amplitudes $\lambda = 0.0$, 0.3, 0.6 and 1.0.

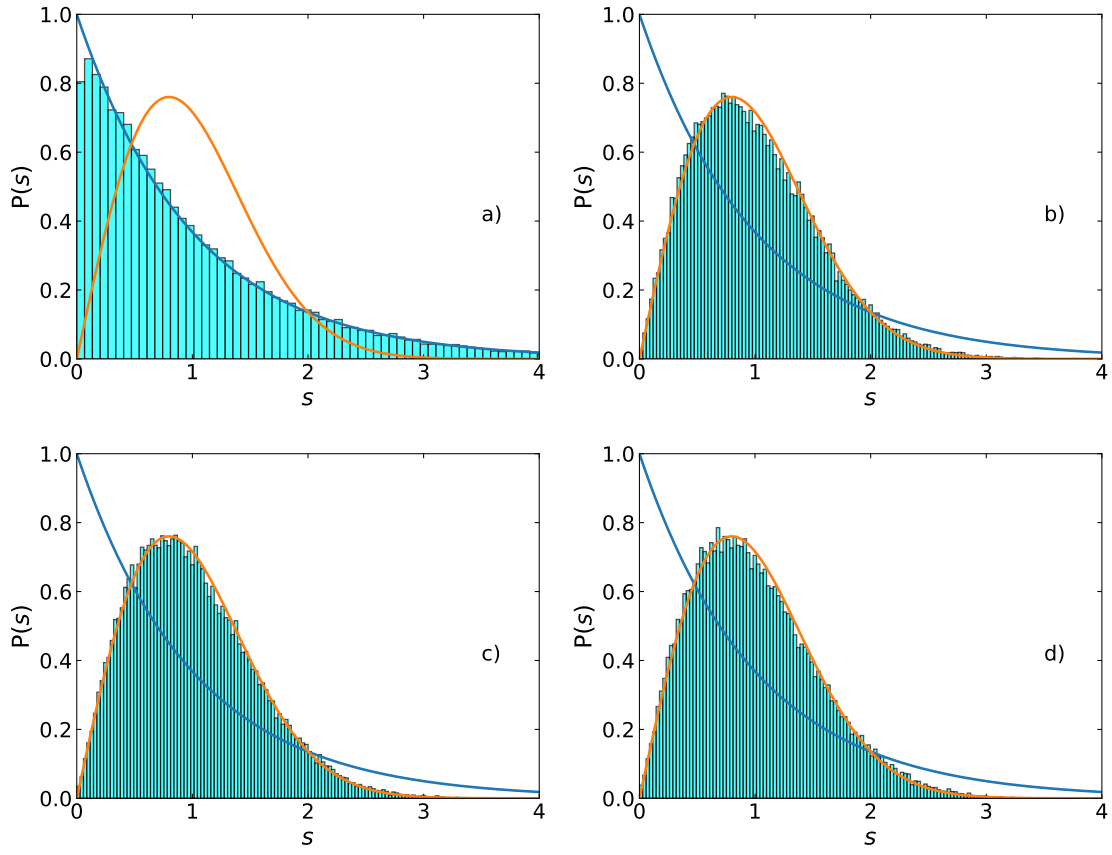

Figure 4.4: Level spacing distribution $P(s)$ for the XXZ model with local perturbation in function of the spacing s. The green line corresponds to the Poisson Eq. (2.10) distribution and the blue line corresponds to the Wigner-Dyson distribution Eq. (2.8). The system size is $L = 16$. Panels correspond to a) $\lambda = 0.0$, b) $\lambda = 0.3$, c) $\lambda = 0.6$ and d) $\lambda = 1.0$.

In figure 4.4 we show the level spacing distribution $P(s)$ for the XXZ model with local perturbations. It is divided into four panels, each panel corresponding to different perturbation amplitudes. In the panels we plot the Poisson distribution (green solid line) and the Wigner-Dyson distribution (blue solid line). Panel (a) corresponds to $\lambda = 0.0$, as we expect the histogram follow the Poisson distribution, which means there are not correlations between energy levels, a signal of integrability. This result is consistent with the prediction provided by $\langle \tilde{r} \rangle$.

Panels (b), (c) and (d) correspond to the perturbation amplitudes $\lambda = 0.3$, 0.6 and 1.0, respectively. Each histogram follows the Wigner-Dyson distribution, which means exits correlations between energy levels, a clear signature of the chaotic behavior of the system. These results are consistent with the predictions given by the study of the $\langle \tilde{r} \rangle$, through the analysis of level spacing distribution we just study short-range correlations and the information given by Fig. 4.4 does not detect relevant differences between panels (a), (b) and (c).

4.3 Level number variance

In this Section we study the level number variance (LNV), denoted by Σ^2. Unlike the mean ratio between consecutive spacings and level spacing distribution which are useful to study short-range correlations between eigenenergies, the LNV is useful to study long-range correlations between eigenenergies. For a Poisson distribution typical of an integrable system, different parts of the spectrum are not correlated, so the LNV is linear with slope one, that is $\Sigma^2(l) = l$, Eq. (2.12). By contrast, in a chaotic system or a random matrix from the GOE level repulsion causes a slow logarithmic increases of the LNV $\Sigma^2(l) \approx \frac{2}{\pi^2} ln(2\pi l)$, Eq. (2.13). This slow growth of the number variance, in comparison with the Poisson statistics, illustrates another spectral signature of chaotic behavior, the spectral rigidity.

Figure 4.5 shows Σ^2 as a function of the interval range l for the system size $L = 16$. It is divided into four panels, each panel corresponds to four different perturbation amplitudes. In the panels, the red dashed line corresponds to the prediction for integrable systems Eq. (2.12), and the blue dashed line corresponds to the chaotic prediction for chaotic systems Eq. (2.13). Panel a) corresponds to $\lambda = 0.0$, when there is no perturbation the system does not present correlations, then the number of eigenenergies fluctuates and the fluctuations increase as the interval size l increases.

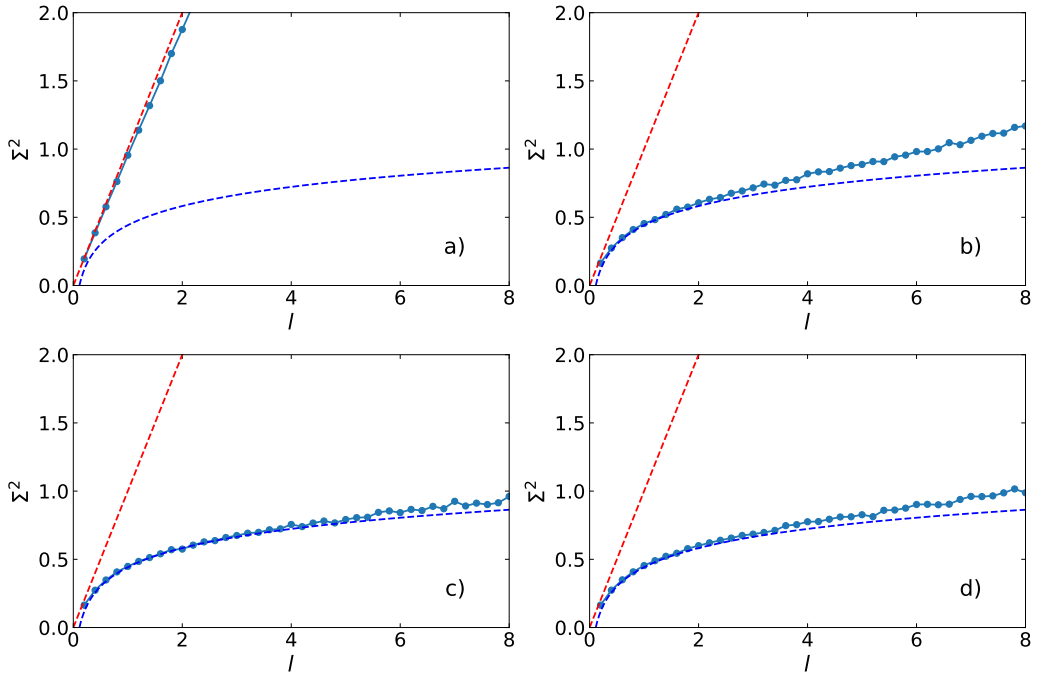

Figure 4.5: Level number variance Σ^2 as function of l for $L = 16$. The red dashed line corresponds to the prediction for integrable systems Eq. (2.12) and the blue dashed line corresponds to the prediction for chaotic systems Eq. (2.13). The perturbation amplitude for each panel is a) $\lambda = 0.0$, b) $\lambda = 0.3$, c) $\lambda = 0.6$ and d) $\lambda = 1.0$.

Panel b) corresponds to $\lambda = 0.3$, the behavior of the Σ^2 has changed abruptly compared with panel a), for the range smaller than $l \approx 2$ the correspondence between the prediction and the numerical results is excellent, however after this interval the numerical results and the prediction separates. Panel c) corresponds to $\lambda = 0.6$, the behavior of the Σ^2 presents an excellent correspondence with the prediction for GOE, even for largest intervals; for the range larger than $l \approx 5$ the numerical results and the prediction separates. Panel c) corresponds to $\lambda = 1.0$, the behavior of the Σ^2 presents a similar behavior to panel b), however for the range larger than $l \approx 4$ the numerical results and the prediction separates.

Since we are working with a physical system we expect that they do not have a complete correspondence between the GOE prediction and the numerical results of the system. The behavior of the Σ^2 shown in panels a), b), c) and d) is in agreement with results already published in the literature, see for instance [27, 20]. In particular, the point where the prediction for GOE and the numerical results separates is known as the Thouless

energy. For eigenenergies smaller than the Thouless energy, the LNV grows logarithmically as GOE. Intuitively, the Thouless energy E_{Th} sets the scale at which the energy levels of the system develop random-matrix-like correlations.

4.4 Inverse participation ratio

In previous sections we studied the spectral statics of the XXZ model with local perturbations, through the study of $\langle \tilde{r} \rangle$ we could identify the regions where the system is integrable or chaotic. Alternatively, there is another approach, Therefore, the study the of eigenstates statistics and structure, in our work we use the IPR as a measure of delocalization or localization and the Porter-Thomas distribution to study the structure of a single eigenstate.

In this section we study the inverse participation ratio for the XXZ model with local perturbations. The IPR gives us information about the degree of localization of a single state. We normalize the IPR_α of a single state using the prediction for GOE systems [36], namely

$$\frac{IPR_\alpha}{\langle IPR_{GOE} \rangle} = \frac{IPR_\alpha (N+2)}{3}. \tag{4.2}$$

If an eigenstate is completely extended then $\frac{IPR_\alpha}{\langle IPR_{GOE} \rangle} = 1$, we refer to these states as ergodic states; on the other hand, for states completely localized $\frac{IPR_\alpha}{\langle IPR_{GOE} \rangle} = \frac{N+2}{3}$. Figure 4.6 shows the IPR_α normalized of each eigenstate as a function of eigenenergy E_α. The figure 4.6 is divided into four panels, each panel corresponds to four different perturbation amplitudes.

Panel a) corresponds to $\lambda = 0.0$, it is possible to note that there are few states completely extended, since most of them have values between 1 and 4 we could say they are extended but not all eigenstates basis participates in the structure of these states, this behavior is expected since for $\lambda = 0.0$ the system is integrable.

Panel b) corresponds to $\lambda = 0.3$, the behavior of the IPR has changed considerably compared to panel a), at the middle of the spectrum most of the states are completely extended; however, at the tails the states did not change their behavior at all. Panel c) corresponds to $\lambda = 0.6$, and the IPR shows a similar behavior to that shown in panel b), although at the middle of the spectrum the width of the IPR fluctuation is smaller than in panel b). Finally, panel d) corresponds to $\lambda = 1.0$, since the system is already in the chaotic regime the IPR shows a behavior similar to panels b) and c).

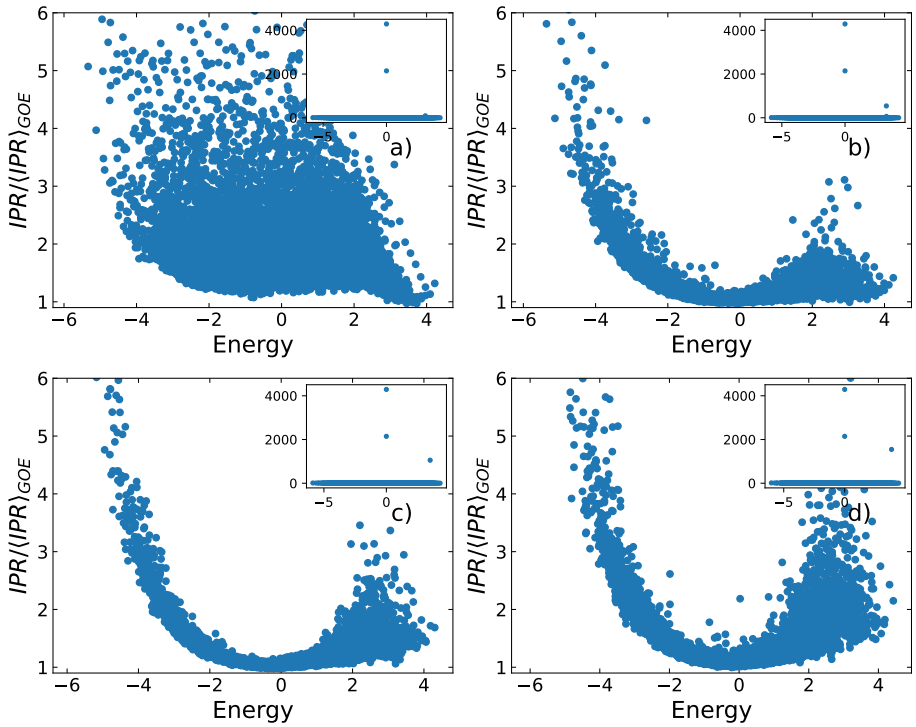

Figure 4.6: IPR for each eigenstate for the XXZ model with local perturbations. For $L = 16$, each panel correspond to the perturbatios amplitudes a) $\lambda = 0.0$, b) $\lambda = 0.3$, c) $\lambda = 0.6$ and d) $\lambda = 1.0$.

As we expected for the systems with the amplitude in the integrable regime most of the eigen state have large normalized IPR, and the system with amplitudes in the chaotic regime present at least at the middle of the spectrum completely extended states, this results are in agreement with result already published [20], and it is possible to claim that for the panels b), c) and d) the system is chaotic. These results are consistent with the results obtained for the energy level statistics analysis.

Another important fact is the information given by the insets, there are states completely localized that remain unchanged even when perturbation is turned on and breaks the integrability of the system. The study of these states is beyond the scope of our work. Finally, the states at the tails practically do not suffer change, they are maintained even in the chaotic regime, this is the part of the reasons why we discarded a percentage on each side of the spectrum to study the spectral properties of the system.

4.5 Porter-Thomas distribution

In this Section we study the Porter-Thomas distribution for the XXZ model with local perturbations, Eq. (4.1). Since the components of a single eigenstates are small we use the continuous random variable transformation to study the distribution of $ln|C_m^n|$ Eq. (2.18). Following the IPR analysis, the most chaotic or extended states are located in the middle of the spectrum, so we decided to analyze the states in this region. We choose a single state in the middle of the spectrum and study its structure.

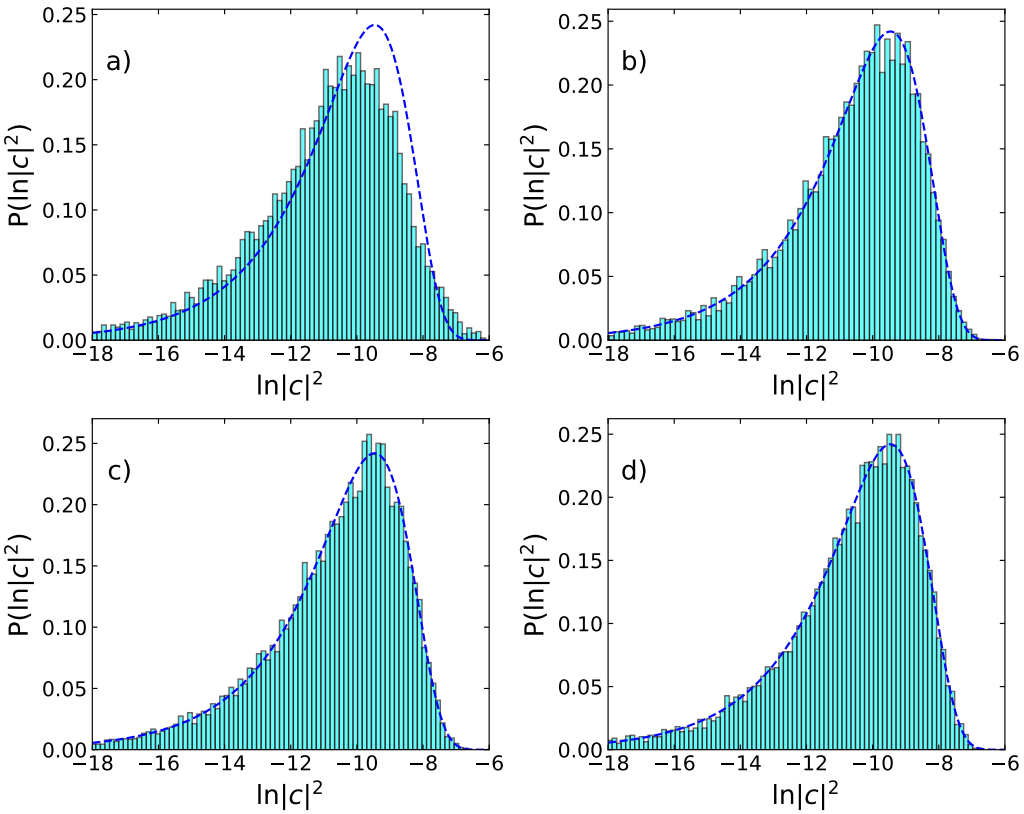

Figure 4.7: Porter-Thomas distribution for the XXZ model with local perturbations, $L = 16$. The perturbation strength for each panel is *a)* $\lambda = 0.0$, *b)* $\lambda = 0.3$, *c)* $\lambda = 0.6$, and *d)* $\lambda = 1.0$. The blue dashed line correspond to the Porter-Thomas distribution Eq. (2.18).

In figure 4.7 we plot the histograms of the weights of a single state for the system size $L = 16$, each panel corresponds to four different perturbation amplitudes. In the panels, the blue dashed line is the Porter-Thomas distribution given by Eq. (2.18). Panel a)

corresponds to $\lambda = 0.0$, as we expected there is a clear deviation between the histogram and the Porter-Thomas distribution, this is a clear indicator that the system is not chaotic, since we expect most of the eigenstates at the middle of the spectrum to behave as a random vector just like eigenstates of matrices from GOE. Panels b), c) and d) correspond to $\lambda = 0.3$, 0.6 and 1.0 respectively. The histograms shown in these panels are in agreement with the Porter-Thomas distribution, which means that the states behave as random vectors.

4.6 Adiabatic gauge potential

4.6.1 The XXZ model

In this Section we use the so-called adiabatic gauge potential (AGP) to prove the integrability of the XXZ model. In order to familiarize with the AGP we reproduce results that are already known. We reproduce the results obtained for the XXZ in [15]. The Hamiltonian is given by:

$$H_{XXZ} = \sum_{i=1}^{L-1} (S^x_{k+1} S^x_k + S^y_{k+1} S^y_k) + \Delta \sum_{i=1}^{L-1} S^z_{k+1} S^z_k. \tag{4.3}$$

We use the same parameters as used in [15], namely, we take anisotropy as the generator of deformations, so $\Delta = \gamma$. Unlike the tools to detect chaos through the spectrum, the AGP does not need dezimitrization i.e. it is possible to work in the complete Hilbert space. Then we study the XXZ model in the complete Hilbert space. To prove the integrability of this system we work with the system sizes $L = 8$, 9, 10, 11, 12, 13 and 14.

$$H_{XXZ}(\gamma) = \sum_{i=1}^{L-1} (S^x_{k+1} S^x_k + S^y_{k+1} S^y_k) + \gamma \sum_{i=1}^{L-1} S^z_{k+1} S^z_k. \tag{4.4}$$

Let be $|\psi_n(\gamma)\rangle$ a base eigenstate of the Hamiltonian $H(\gamma)$ so $H(\gamma)|\psi_n(\gamma)\rangle = E_n(\gamma)|\psi_n(\gamma)\rangle$. On the other hand

$$\frac{\partial H(\gamma)}{\partial \gamma} = \sum_{i=1}^{L-1} S^z_{k+1} S^z_k. \tag{4.5}$$

Let be $|\psi_l\rangle$ a base eigenstate of $\partial_\gamma H(\gamma)$ so $\partial_\gamma H(\gamma)|\psi_l\rangle = E_l|\psi_l\rangle$. We can expand the base elements $|\psi_n(\gamma)\rangle$ of the Hamiltonian $H(\gamma)$ in terms of the base elements $|\psi_l\rangle$ of $\partial_\gamma H(\gamma)$ as

$$|\psi_n(\gamma)\rangle = \sum_l \langle\psi_l|\psi_n(\gamma)\rangle|\psi_l\rangle = \sum_l C_{nl}|\psi_l\rangle. \tag{4.6}$$

Where $\langle\psi_l|\psi_n(\gamma)\rangle = C_{nl}$. Therefore

$$\langle\psi_n(\gamma)|\partial_\gamma H|\psi_m(\gamma)\rangle = \left(\sum_l C^*_{nl}\langle\psi_l|\right)\sum_{i=1}^{L-1} S^z_{k+1}S^z_k\left(\sum_k C_{nk}|\psi_k\rangle\right)$$

$$= \sum_l\sum_k C^*_{nl}C_{nk}\langle\psi_l|\sum_{i=1}^{L-1} S^z_{k+1}S^z_k|\psi_k\rangle. \tag{4.7}$$

Finally, we can express the AGP as

$$\|\mathscr{A}_\gamma\|^2 = \frac{1}{\mathscr{D}}\sum_n\sum_{m\neq n}\frac{\omega^2_{mn}}{(\omega^2_{mn}+\mu^2)^2}|\sum_l\sum_k C^*_{nl}C_{nk}\langle\psi_l|\sum_{i=1}^{L-1} S^z_{k+1}S^z_k|\psi_k\rangle|^2 \tag{4.8}$$

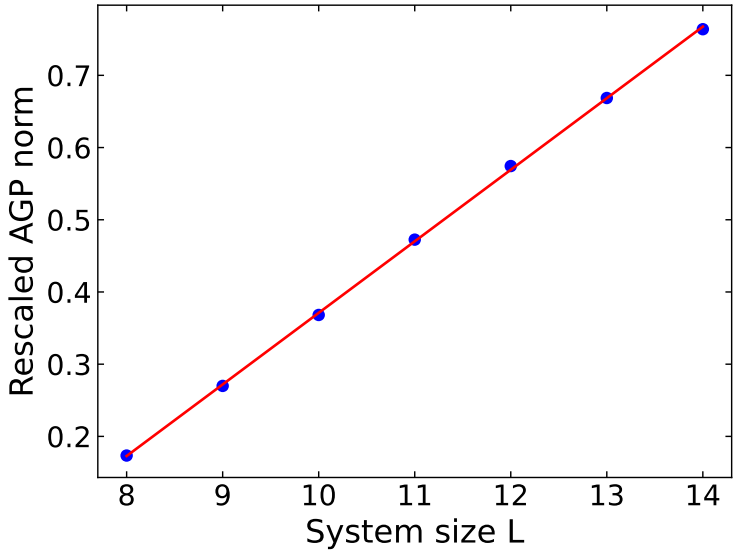

Figure 4.8: Rescaled AGP norm $\|\mathscr{A}\|^2/L$ for the XXZ model with $\Delta = 1.1$. The red solid line is an adjust of a first order polynomial given by $\|\mathscr{A}\|^2/L = 0.0991L - 0.61$.

Figure 4.8 shows the results obtained for the AGP for the XXZ model Eq. (4.4) as a function of the system size. The red solid line is the fitting to the data using a polynomial function. The AGP presents a polynomial behavior which means that the XXZ is an integrable model. The scaling $\|\mathscr{A}\|^2/L = 0.09910139L - 0.61998375$ was found, this result is consistent with that reported in literature [15], the polynomial scale reported is $\|\mathscr{A}_{int}\|^2/L = 0.09L - 0.56$.

Once we are familiarized with the AGP, we study the XXZ model considering the parameters values used in this work, namely we use the anisotropy value $\Delta = 0.48$. In the

subsequent work, we worked in the half-filling sector. On the other hand, the AGP norm just gives us a point for each system size then we decide extend our study to the system sizes L = 8, 9, 10, 11 , 12, 13, 14, 15 and 16. Then we calculate the AGP norm given by Eq. (5.5) for this new anisotropy value.

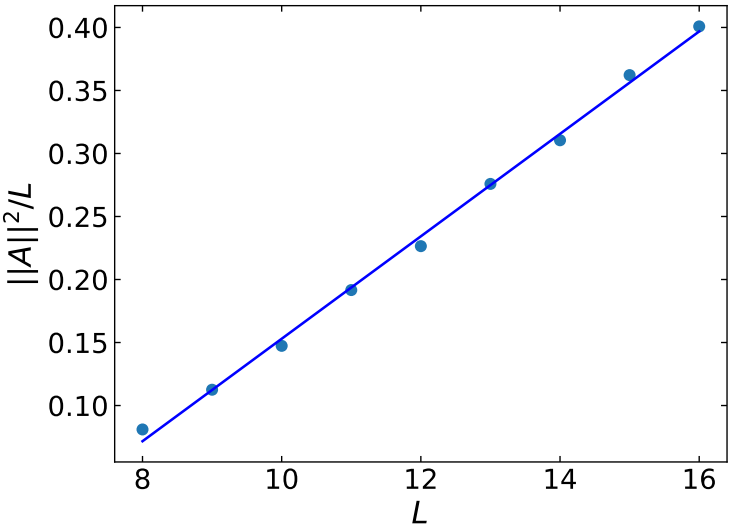

Figure 4.9: Rescaled AGP norm $\|\mathscr{A}\|^2/L$ for the XXZ model with $\Delta = 0.48$. The blue solid line is the fitting given by $\|\mathscr{A}\|^2/L = 0.04064L - 0.25349$.

Figure 4.9 shows the results obtained for the AGP as a function of system size. The blue solid line is the fitting to the data using a polynomial function. As expected, the AGP displays polynomial behavior, a clear signature of the system integrability, the polynomial fitting is given by $\|\mathscr{A}\|^2/L = 0.04064L - 0.25349$.

4.6.2 The XXZ model with local perturbations

In this Section we investigate the effect of the impurities at the edges of the chain. We decide to add one defect at the beginning of the chain and vary its amplitude, the results are presented in Appendix A. We fix the amplitude at the beginning of the chain to $\epsilon_1 = 0.001$, since this amplitude does not change the scaling of the AGP. The next step is to investigate the effect of adding another impurity at the end of the chain. The final Hamiltonian that we are going to study is

$$H_\epsilon = \sum_{k=1}^{L-1} (S_k^x S_{k+1}^x + S_k^y S_{k+1}^y + \Delta S_k^z S_{k+1}^z) + \epsilon_1 S_1^z + \epsilon_L S_L^z. \tag{4.9}$$

From Appendix A we know that the Hamiltonian exhibits the polynomial behavior for the anisotropy value $\Delta = 0.48$ and $\epsilon_1 = 0.001$, then we still take the anisotropy as the generator of deformations $\gamma = \Delta$. We vary the impurity amplitude at the end of the chain ϵ_L.

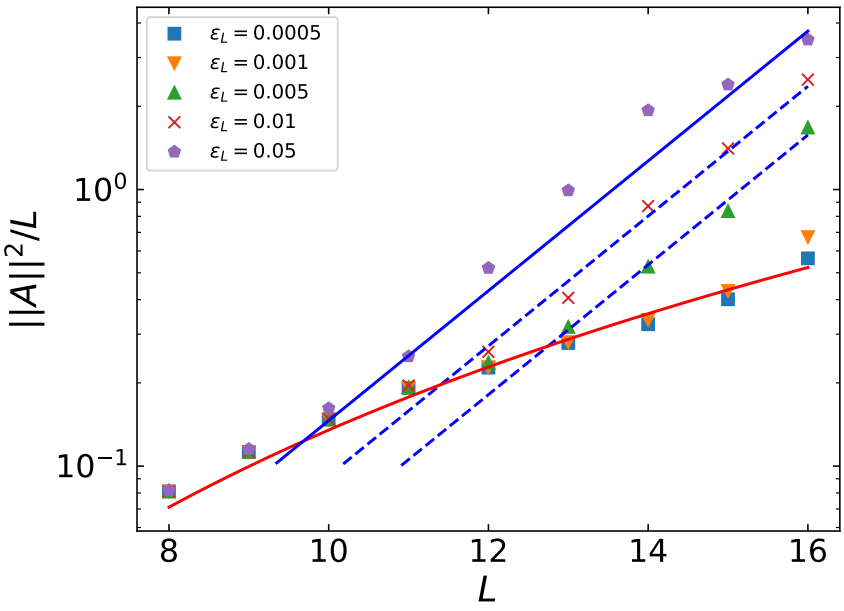

Figure 4.10: Rescaled AGP norm $||\mathscr{A}||^2/L$ for the XXZ model with local perturbations at the edges and $\Delta = 0.48$. The solid red line is the fitting given by $||\mathscr{A}||^2/L = 0.00017L^{2.87}$. The solid blue line is the adjustment given by $||\mathscr{A}||^2/L = 0.25e^{0.54L}$

Figure 4.10 shows the rescaled AGP as a function of the system size on semi-log scale. We vary the amplitude of ϵ_L, we choose five different amplitudes (see the chart legend). The solid red line is the fitting given by $||\mathscr{A}||^2/L = 0.00017L^{2.87}$. The solid blue line is the fitting given by $||\mathscr{A}||^2/L = 0.25e^{0.54L}$. The behavior of the AGP depicted in this figure was unexpected since we expected fluctuations around the red solid line, however, it presents a transition for large amplitudes. Naturally, the question of the integrability breaking emerges, is this a signal of chaos? since the AGP norm scales as an exponential.

In the work [15] a simple calculation was done to know what is the exponent expected for systems that present chaotic behavior the prediction is $||\mathscr{A}||^2/L \sim e^{log(2)L}$ and it was found that there exists another limit where $||\mathscr{A}||^2/L \sim e^{2log(2)L}$. Then according to this information the exponent found for this system $\kappa = 0.54$ is smaller than the range for chaotic systems $[0.69, 1.38]$. However, there are no works yet that supports this assumption. A more

detailed study of this AGP behavior and its consequences is left for future works, probably a study using ensembles of random matrix theory could help to clarify this problem.

4.6.3 The transition of the XXZ model

In this Section we study the transition from the integrable regime to the chaotic regime through the AGP analysis. The first step of our work is to establish the amplitude of the impurities at the edges of the chain, in the previous section we found that there are amplitudes that change the scaling of the AGP norm. Since we are interested in the transition and find the crossover points between the polynomial scaling and the exponential scaling, we choose amplitudes that do not change the scaling of the AGP. The chosen amplitudes are $\epsilon_{1,L} = 0.001$. Then we add the perturbation at the middle of the chain and we vary its amplitude. The Hamiltonian implemented is given by Eq. (3.10) that we repeat here

$$H_{[1/2]} = \sum_{k=1}^{L-1} (S_k^x S_{k+1}^x + S_k^y S_{k+1}^y + \Delta S_k^z S_{k+1}^z) + \epsilon_1 S_1^z + \lambda S_{L/2}^z + \epsilon_L S_L^z.$$

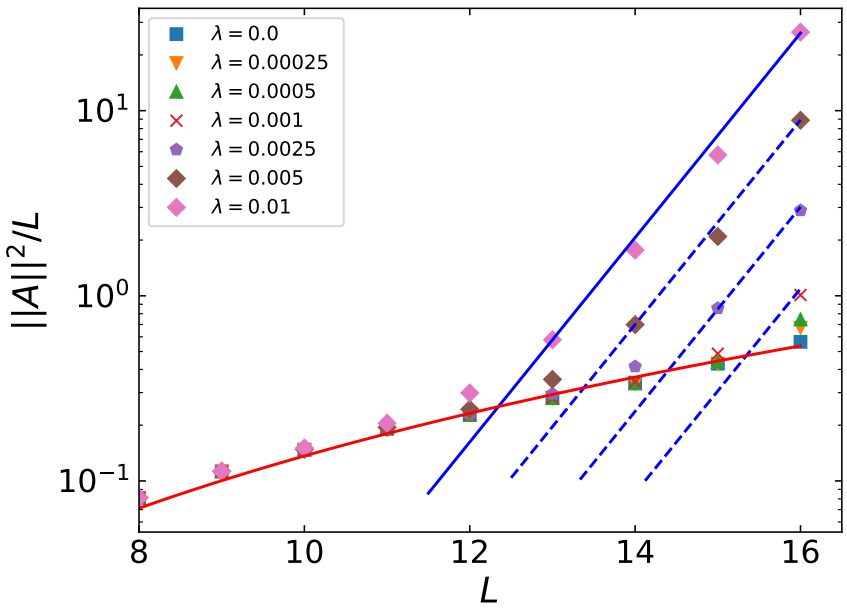

Figure 4.11: Rescaled AGP norm $||\mathscr{A}||^2/L$ for the XXZ model with local perturbations at the edges and $\Delta = 0.48$. The solid red line is the fitting given by $||\mathscr{A}||^2/L = 0.00017L^{2.913}$. The solid blue line is the adjustment given by $||\mathscr{A}||^2/L \sim e^{1.27L}$

The figure 4.11 shows the rescaled AGP norm for the XXZ model with local perturbations, we present it in semi-log scale. We vary the amplitude of λ and choose seven different amplitudes (see the chart legend). The blue solid line is an exponential fitting given by $||\mathscr{A}||^2/L \sim e^{1.27L}$. The red solid line is a polynomial law fitting given by $||\mathscr{A}||^2/L = 0.0003L^{2.913}$. The blue squares are for $\lambda = 0.0$, the effect of adding the perturbation at the end of the chain is that the fitting is no more like a single defect, where we found the fitting $||\mathscr{A}||^2/L = 0.00017L^{2.87}$. Now the best fitting is given by $||\mathscr{A}||^2/L = 0.0003L^{2.913}$, as is expected for integrable systems, then for amplitudes of the defect at the edges smaller than $\epsilon = 0.001$ the AGP norm behaves as a polynomial law.

For the larger amplitude analyzed $\lambda = 0.01$, the change in the behavior is evident, for small system size the AGP norm follows the same behavior as for an integrable systems, however there are system sizes for which the AGP changes its behavior, in this case $L > 12$, after this system size the AGP present a completely different behavior that follows the $||\mathscr{A}||^2/L \sim e^{1.27L}$ scaling, the exponent found is $\kappa = 1.27$ which is in the interval $[0.69, 1.38]$, so the system clearly shows a transition from the integrable regime to the chaotic regime. Another important fact is that we found the same exponent that the exponent found in the work [15], however in that work it was claimed that the exponent has a dependence on the anisotropy value. Then another question emerges, does the exponent depend on the anisotropy amplitude?.

Finally, is clear that the change of the AGP scaling depends on system size, since for small perturbation amplitudes we need to reach large system sizes to break the integrability of the system, this is in agreement with our result in previous section, in particular the results of $\langle \tilde{r} \rangle$ where is clear the dependence on system size.

Figure 4.12 depicts the amplitude needed to break the integrability of the system λ as function of the system size. We present it in semi-log scale. The red solid line is an exponential fitting given by $\lambda = 62.76e^{-0.7L}$. The blue squares are the crossover points between the integrable behavior (red line in figure 4.11) and the chaotic behavior (blue lines in Fig. 4.11).

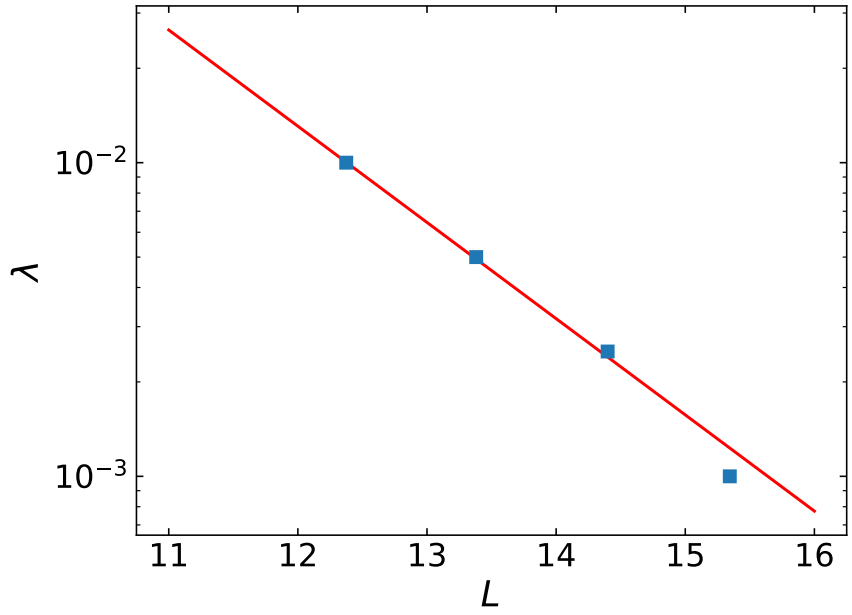

Figure 4.12: Amplitude λ of the defect at the middle od the chain needed to break the integrability of the system as function of system size L. The blue square are the crossover points. The red solid line is the fitting given by $\lambda = 62.76e^{-0.7L}$.

In this Chapter we use the ratio between consecutive spacings $\langle\tilde{r}\rangle$ to have a more clearly perspective of the general behavior of the XXZ model with local perturbations. This quantity help us to choose different amplitudes of λ and analyze them with the other tools from RMT. The information given by the level spacing distribution is in agreement with the results obtained by $\langle\tilde{r}\rangle$, when the perturbation λ is turned off the system is in the integrable regime and there are not correlations between eigenenergies, therefore the histogram has an excellent correspondence with the Poisson distribution. On the other hand, when $\lambda > 0.1$ the system is in the chaotic regime, then the histogram has an excellent correspondence with the Wigner-Dyson distribution. On the other hand, the level number variance helps us to know the rigidity of the spectrum, the rigidity of the energy spectrum means that the deviations of the energy levels from those of a local uniform spectrum are generally small.

The study of the IPR provides additional information about the system, in particular when the system is in the integrable regime more of the states are localized. When the system is in the chaotic regime, the states at the middle of the spectrum are extended. The agreement between the distribution of energy eigenstates components and the Porter-

Thomas distribution means that the energy eigenstates in the chaotic regime behave as uncorrelated random vector with a Gaussian distribution.

We reproduced results published in the work [15]. The AGP shows a remarkable sensitive to detect chaos and we obtained a relation between the system size and the amplitude λ to predict the emerge of chaos. We found that the impurities at the edges of the chain could change the scaling of the AGP, however a more detailed analysis is required to understand the reason. For instance, the prediction for the onset of chaos given by the AGP for a system with $L = 16$ spins is $\lambda = 0.00085$, meanwhile the $\langle \tilde{r} \rangle$ predicts that the system is in the chaotic regime for $\lambda = 0.15$.

Chapter 5

The interacting Aubry-André model

The implemented Hamiltonian is given by Eq. (3.12) which we repeat here

$$H = H_{\mathrm{XXZ}} + \sum_{k=1}^{L} \lambda \cos(2\pi k\beta + \phi) S_k^z. \tag{5.1}$$

Where we choose to work with number of particles $L = 8, 10, 12, 14, 16$. For each system size we vary the perturbation strength in the interval $[0, 3.0]$ using steps of 0.1, we do this to characterize the transition from the integrable regime to the chaotic regime. We choose six perturbation amplitudes λ since we are interested in characterizing the behavior in the different zone, the chaotic zone, the intermediate zone, and the localize zone. We analyze the system using standard methods to detect chaos. The chosen values are $\lambda = 0.1$, 0.5, 0.8, 1.1, 1.4 and 2.0. We diagonalize the Hamiltonian for each system size and for each value of λ.

Since our study is numeric, it is important to have a large sample space. However, this is not possible for the smallest system sizes L. Therefore, we fix this problem by making an ensemble that extends the sample space for the smallest system sizes L where we consider the phase ϕ as a random number. The phase ϕ takes random values in the range $[0, 2\pi]$. The ensembles for the system sizes $L = 8$, 10 and 12 are 1000 realizations, and for the largest system sizes $L = 14$ and 16 the ensemble are just 10 realizations. To have an average for the different spectral properties, first we calculated the property for each realization, and then we averaged for the entire ensemble. For instance, to calculate the level spacing distribution

we fix the bins of the histogram and then we averaged the histogram for all realizations. For the ratios between consecutive spacings, we calculated them for each realization and then averaged them for the entire ensemble.

5.1 Mean ratio between consecutive spacings

In this section, we present the results obtained for the mean ratio between consecutive spacings $\langle \tilde{r} \rangle$ for the Aubry-André model, we present the results for the six different system sizes $L = 8$, 10, 12, 14, and 16.

In the Fig. 5.1 we plot the $\langle \tilde{r} \rangle$ for different system sizes as a function of the Harper potential amplitude λ. The figure is divided into six panels, each panel belongs to a different system size. The blue solid line in each graph is the prediction for chaotic systems or matrices belonging to the GOE $\langle \tilde{r} \rangle = 0.53590$, the red solid line is the prediction for integrable systems $\langle \tilde{r} \rangle = 0.38629$.

Panel a) corresponds to the system size $L = 8$, there we see that the system reach the chaotic regime approximately for $\lambda = 0.5$, however practically intermediately the system begins to move to the localized regime, however it looks like the system does not stay in the localized regime because there are a lot of fluctuations, we attribute this behavior to finite size effects.

Panel b) corresponds to the system size $L = 10$, the transition from the integrable regime to the chaotic regime is faster than the systems size $L = 8$, however it is not possible to claim that the system remains in the chaotic regime for $\lambda \approx 0.4$. Approximately for $\lambda > 0.8$ the systems transitions to the localized regime, nevertheless our result shows a lot of fluctuations for $\lambda > 1.5$, it is not possible to claim wether the system is localized or shows another kind of behavior. Panel c) corresponds to system size $L = 12$, the transition from the integrable regime to the chaotic is faster than the other two system sizes $L = 8$, 10; it is necessary to note that the system does not reach the prediction for GOE matrices, it is close to the blue line. The transition from the chaotic regime to the localize regime stars after $\lambda > 0.7$, the system is in the localized regime around $\lambda \approx 2.5$. The panel d) corresponds to the system size $L = 14$, here it is clear that the transition is faster as the system size increases. The transition starts approximately at $\lambda > 0.8$ and reaches the localized regime approximately for $\lambda > 2.2$. Finally, panel e) corresponds to the system size $L = 16$, this system presents the fastest transition and the systems reach the localized

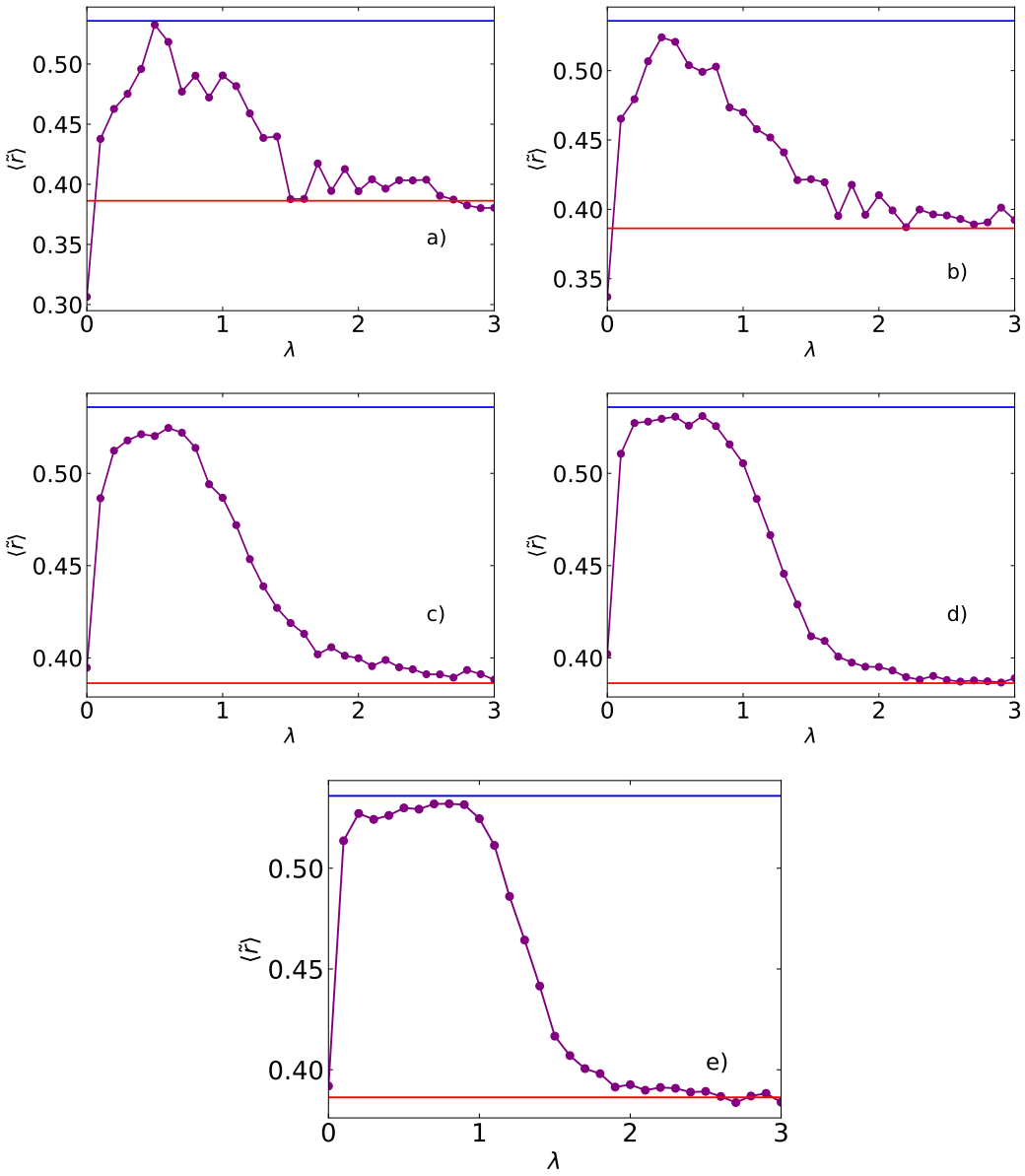

Figure 5.1: Mean ratio between consecutive spacings $\langle \tilde{r} \rangle$ in function of the perturbation amplitude λ for the interacting Aubry-André model for different systems sizes. The blue line corresponds to the prediction for chaotic systems, $\langle \tilde{r} \rangle \approx 0.53590$ and the red line corresponds for integrable systems, $\langle \tilde{r} \rangle \approx 0.38629$. The system sizes are a) $L = 8$, b) $L = 10$, c) $L = 12$, d) $L = 14$ and e) $L = 16$.

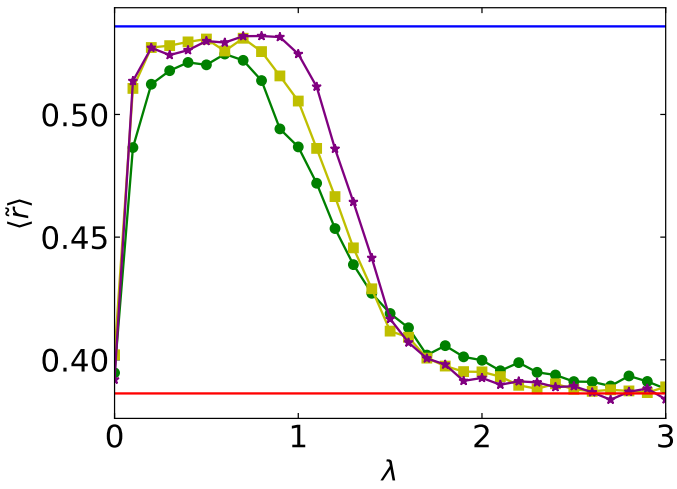

Figure 5.2: Mean ratio between consecutive spacings $\langle \tilde{r} \rangle$ in function of the perturbation amplitude λ for three different system sizes $L = 12$, 14 and 16. The green circles are for $L = 12$, the yellow squares are for $L = 14$ and the purple stars are for $L = 16$. The blue line corresponds to the prediction for chaotic systems, $\langle \tilde{r} \rangle \approx 0.53590$ and the red line corresponds to integrable systems, $\langle \tilde{r} \rangle \approx 0.38629$.

regime approximately for $\lambda > 1.9$.

In order to expose the dependence of the mean ratio $\langle \tilde{r} \rangle$ on the system size, in Fig. 4.3 we plot the $\langle \tilde{r} \rangle$ for the system sizes $L = 12$, 14 and 16. The green circles correspond to system size $L = 12$, the yellow squares correspond to system size $L = 14$ and the purple stars correspond to system size $L = 16$. In this figure we can see how the transition depends on the system size, the transition is faster as the system size increases. We expect that for sufficiently large system sizes only an infinitesimal perturbation amplitude λ is needed enough to break the integrability of the system. The chaotic zone is more extended for largest system sizes and the transition looks faster, the largest system reach the localized regime faster too. This is interesting because it is clear that the transition from the integrable regime to the chaotic regime depends on the system size, according to these results the transition begins first for the larger systems than for the smaller systems.

5.2 Level spacing distribution

In this Section we study the level spacings distribution $P(s)$ for the interacting Aubry-André model, following the XXZ model analysis we use the same unfolding, namely we use a polynomial fitting of 7th order. We report only the results obtained for $L = 16$ since the level spacing distribution is a statistical study and this system has the largest statistical sample. We choose six different Harper potential amplitudes, the chosen amplitudes are localized in different regions according to the results obtained by $\langle \tilde{r} \rangle$, $\lambda = 0.1$, 0.5, 0.8, 1.1, 1.4 and 2.0.

Figure 5.3 shows the level spacing distribution $P(s)$. It is separate into six panels, each one corresponds to a different Harper potential amplitude. In the panels, we plot the Poisson distribution (green solid line) and the Wigner-Dyson distribution (blue solid line). Panel a) corresponds to $\lambda = 0.1$, according to the analysis of $\langle \tilde{r} \rangle$, for this amplitude the system does not reach the chaotic regime, the information given by the $P(s)$ the states repeal each other; however it is not possible say that the systems present the Wigner-Dyson distribution.

Panels b) and c) belong to $\lambda = 0.5$ and 0.8 respectively, the match between the histogram and the Wigner-Dyson distribution is quite good, it is possible to say that the system is chaotic, this is in agreement with the results obtained through $\langle \tilde{r} \rangle$. The panel d) corresponds to $\lambda = 1.1$, is possible to note that for short distance $s < 1$ the levels repeal between them, however the histogram does not follow the Wigner -Dyson distribution, this is in agreement with the information given by the study of $\langle \tilde{r} \rangle$. The panel e) corresponds to $\lambda = 1.4$, the histogram shows an intermediate behavior but closer to the Poisson distribution and the Wigner-Dyson distribution. Finally, panel f) corresponds to $\lambda = 2.0$, the histogram follows the Poisson distribution, a clear indicator that the system is integrable and there are not correlations between energy eigenvalues.

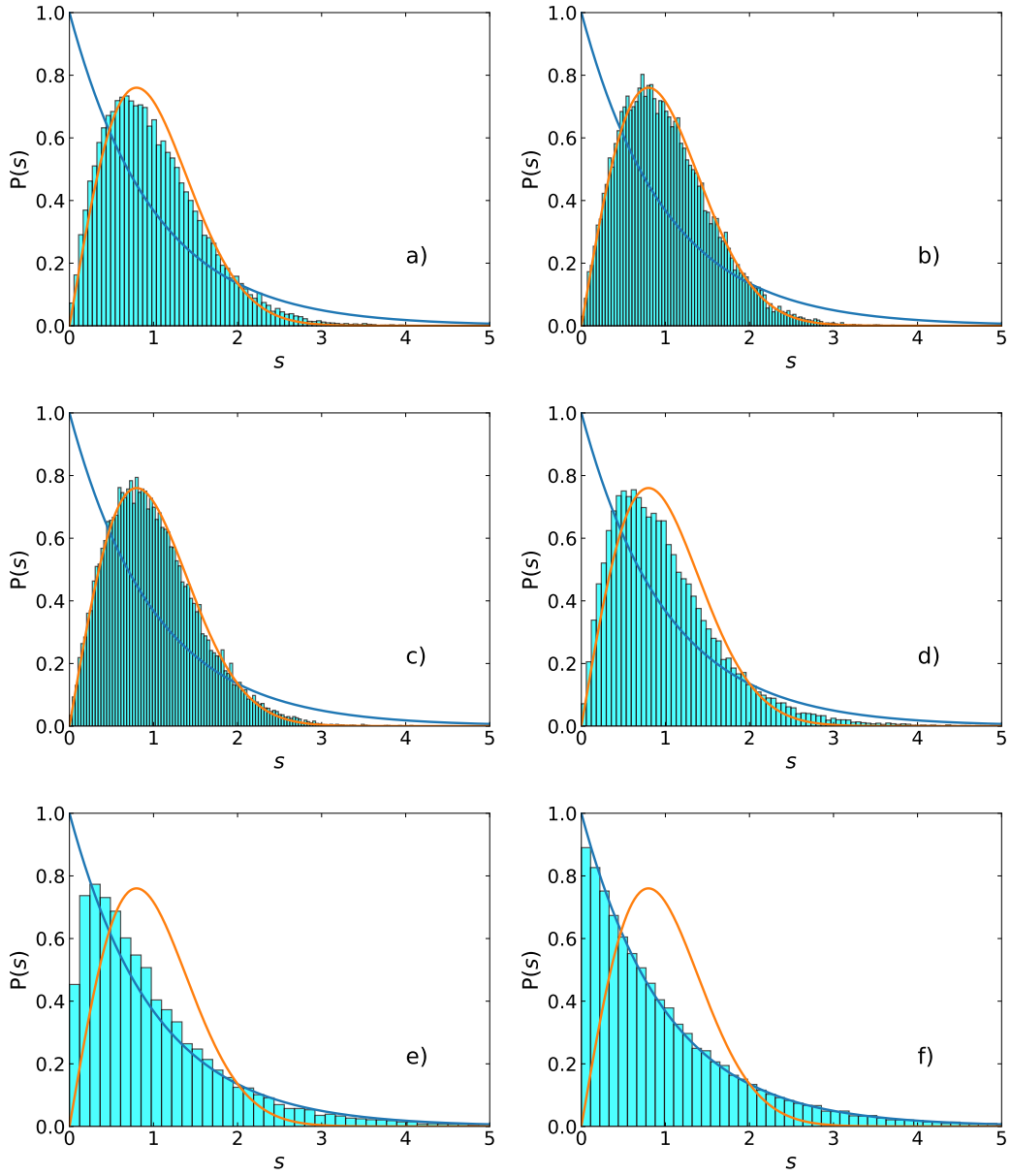

Figure 5.3: Level spacing distribution $P(s)$ in function of the spacing s. the red line corresponds to the Poisson distribution Eq. (2.10) and the blue line corresponds to the Wigner-Dyson distribution Eq. (2.8). The system size is $L = 16$. The perturbation amplitude λ for each graph is a) 0.1, b) 0.8, c) 1.4 and d) 2.0.

5.3 Level number variance

In this section, we study the level number variance Σ^2 for the interacting Aubry-André model. Figure 5.4 shows the results obtained for Σ^2 as function of length l. It is separate into six panels, each one displays the Σ^2 for different potential amplitudes. It is plotted the Σ^2 for integrable systems (red dashed line) Eq. (2.12) and the Σ^2 for chaotic systems (the blue dashed line) Eq. (2.13). The Panel a) corresponds to the amplitude $\lambda = 0.1$. According to $\langle \tilde{r} \rangle$, the system is close to the chaotic regime predicted for GOE matrices, the information given by the Σ^2 it that just for $l < 2$ the spectrum behaves like a matrix of RMT.

Panel b) corresponds to $\lambda = 0.5$, the results for this value of λ are quite interesting because the correspondence between the results obtained and the prediction for chaotic systems predicted for GOE matrices continues even for a long-range $l \approx 8$, then the spectrum behaves as a system described by RMT even for long range correlations. Panel c) corresponds to $\lambda = 0.8$, although the study of short range correlation through the $\langle \tilde{r} \rangle$ and $P(s)$ say that the system is described by RMT, the information given by Σ^2 tell us that this description is just for short range, namely just short energy range are correlated between them.

Panel d) corresponds to the Harper potential amplitude $\lambda = 1.1$, the information obtained through the study of short-range correlations indicates that the system is close to the chaotic regime predicted for GOE matrices; however, the information given by the Σ^2 suggests that the correlations are just for short ranges $l < 0.8$. The panel e) corresponds to $\lambda = 1.4$, the results obtained suggest that the system is closer to an integrable system tham to a chaotic one, this is in agreement to the previous results. Finally, panel f) corresponds to $\lambda = 2.0$, there is an excellent correspondence between the results obtained for Σ^2 and the prediction for integrable systems, which is in agreement with the result obtained through the $\langle \tilde{r} \rangle$ and $P(s)$.

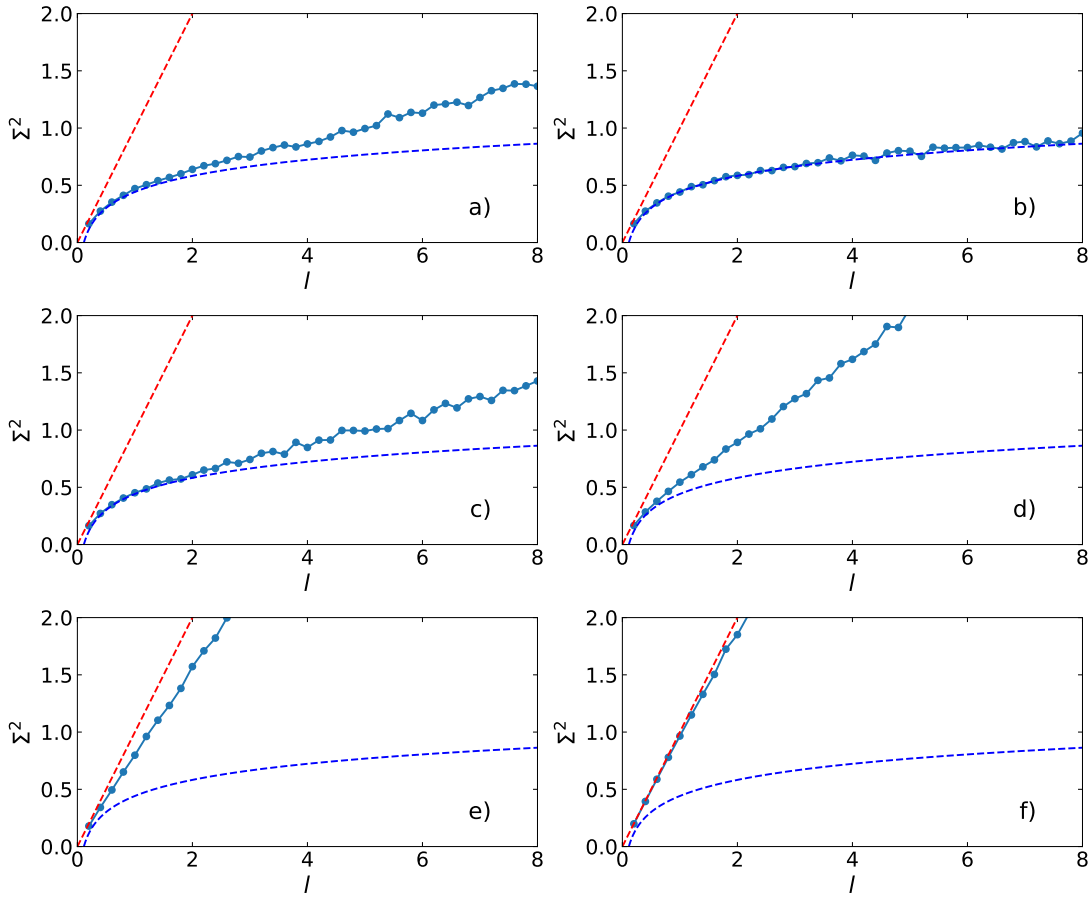

Figure 5.4: Level number variance Σ^2 for the interacting Aubry-André model in function of l for $L = 16$. The red line corresponds to integrable systems Eq. (2.12) and the blue line corresponds to GOE Eq. (2.13). The perturbation amplitude λ for each graph is a) 0.1, b) 0.5, c) 0.8, d) 1.1, e) 1.4 and d) 2.0.

5.4 Inverse participation ratio

In this Section we study the inverse participation ratio of eigensates for the Aubry-André model. As was mentioned in section (2), the IPR measures the localization degree of a single state. We normalize the IPR_α using the prediction for GOE systems [36], namely

$$\frac{IPR_\alpha}{\langle IPR_{GOE}\rangle} = \frac{IPR_\alpha(N+2)}{3}. \tag{5.2}$$

If an eigenstate is completely extended as eigenstates of GOE matrices then $\frac{IPR_\alpha}{IPR_{GOE}} = 1$, we refer to these states as ergodic states; on the other hand, for states completely localized

$\frac{IPR_\alpha}{IPR_{GOE}} = \frac{N+2}{3}$. Figure 5.5 shows the normalize IPR_α of each eigenstates as function of the eigenenergy E_α. We present six panels, each panel corresponds to a different Harper potential amplitude. Panel a) corresponds to $\lambda = 0.1$, it is possible to note that at the middle of the spectrum most of the eigenstates are extended since $IPR_\alpha/IPR_{GOE} < 2$, there are states that stand out from the main group namely there are states more localized, on the other hand the tail shows a completely different behavior, the left tail has more localized states than the right tail, finally the inset shows the $\frac{IPR_n}{IPR_{GOE}}$ complete, it is interesting because there are two eigenstates completely localized at the middle of the spectrum.

Panel b) corresponds to $\lambda = 0.5$, the behavior of the IPR changes, there are more states localized at the tails, specially in the right tail; however, at the middle of the spectrum most of the states are extended, nevertheless another localized states emerge in this zone, these states are known as scars [56, 57]. It is important to note that there are three states completely localized at the middle of the spectrum, the study of these states are outside the scope of our work. Panel c) corresponds to $\lambda = 0.8$, the $\frac{IPR_\alpha}{IPR_{GOE}}$ has changed the behavior abruptly compared to panels a) and b), there are many localized states across the spectrum; unlike the information given by the $\langle\tilde{r}\rangle$, it predicts the system is chaotic, the information given by the $\frac{IPR_\alpha}{IPR_{GOE}}$ suggests the system is not chaotic, then the $\langle\tilde{r}\rangle$ is not sensitive enough and probably it is need to reach higher dimensions to have better information of the system ; the inset shows the complete $\frac{IPR_\alpha}{IPR_{GOE}}$.

Panel d) corresponds to $\lambda = 1.1$, here it is clear that most of the states are localized, according to the information given by the $\langle\tilde{r}\rangle$ the system stays in an intermediate phase. Panel e) corresponds to $\lambda = 1.4$, for this amplitude the $\frac{IPR_\alpha}{IPR_{GOE}}$ of the states in the center of the spectrum is greater than that of states in the same energy region for the other four amplitudes λ analyzed; this means that the states are more localized and less basis states participate in the structure of these eigenstates. Finally, panel f) corresponds to $\lambda = 2.0$, in this plot it is more clear that the states are more localized which is in agreement with the prediction from $\langle\tilde{r}\rangle$ since for $\lambda = 2.0$ the system stays in the localized regime.

A final comment on the states completely localized at the middle of the spectrum, these states are quite interesting because they maintained unchanged for the different Harper potential amplitudes λ, the study of these states are outside the objectives of this work, so it remains as a topic to be studied in future works.

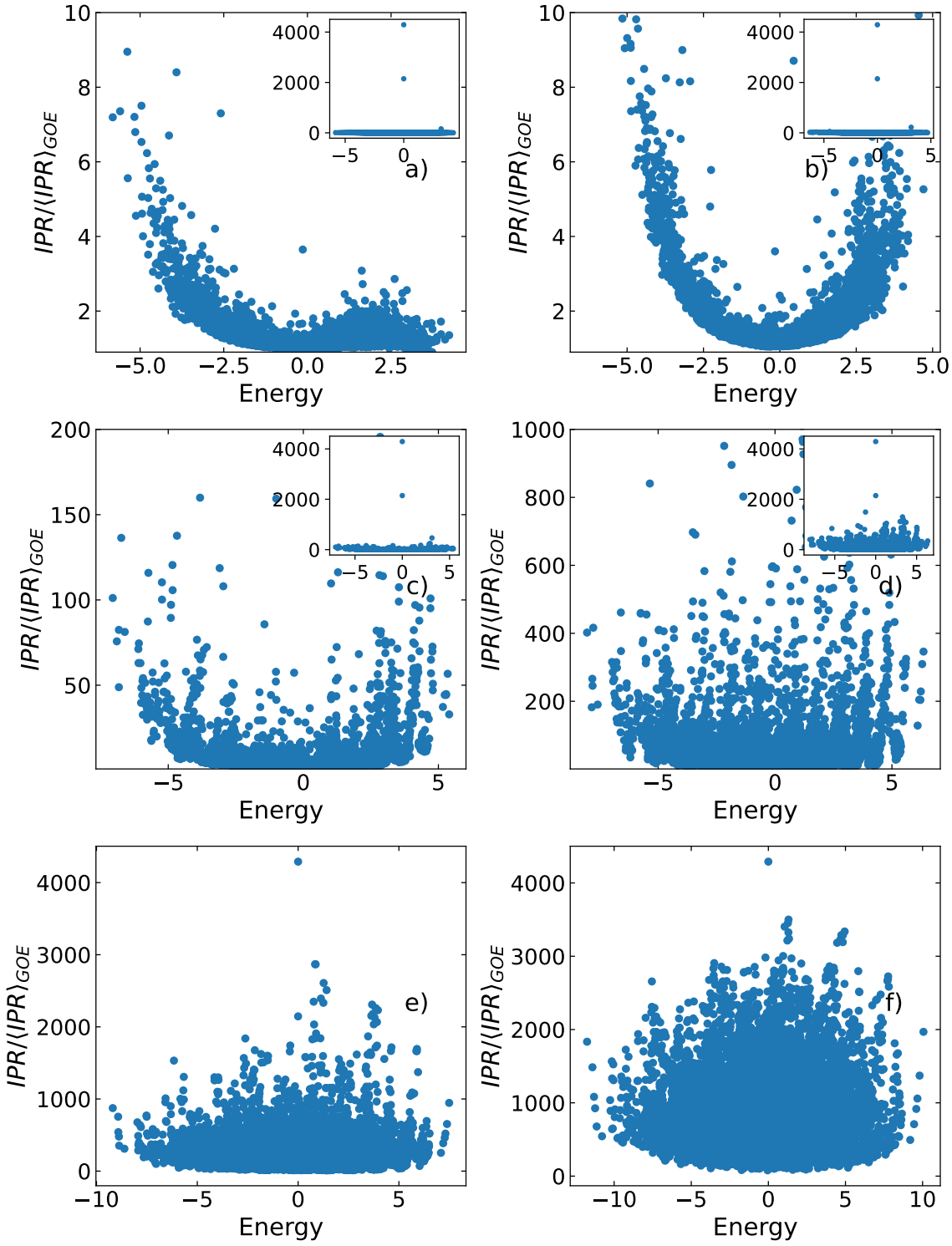

Figure 5.5: IPR for each eigenstate of the interacting Aubry-André model. For $L = 16$, the perturbation amplitude for each panel is a) 0.1, b) 0.8, c) 1.4 and d) 2.0.

5.5 Porter-Thomas distribution

In this section we study the Porter-Thomas distribution for the Aubry-André model. In figure 5.6 we plot the histogram of components $|c_n^\alpha|$ of a single state for the system size $L = 16$, we choose an eigenstate $|\psi_\alpha\rangle$ located in the middle of the spectrum. We present six panels in Fig. 5.6, each one corresponds to six different perturbation amplitudes. In the panels the blue dashed line is the Porter-Thomas distribution given by Eq. (2.18).

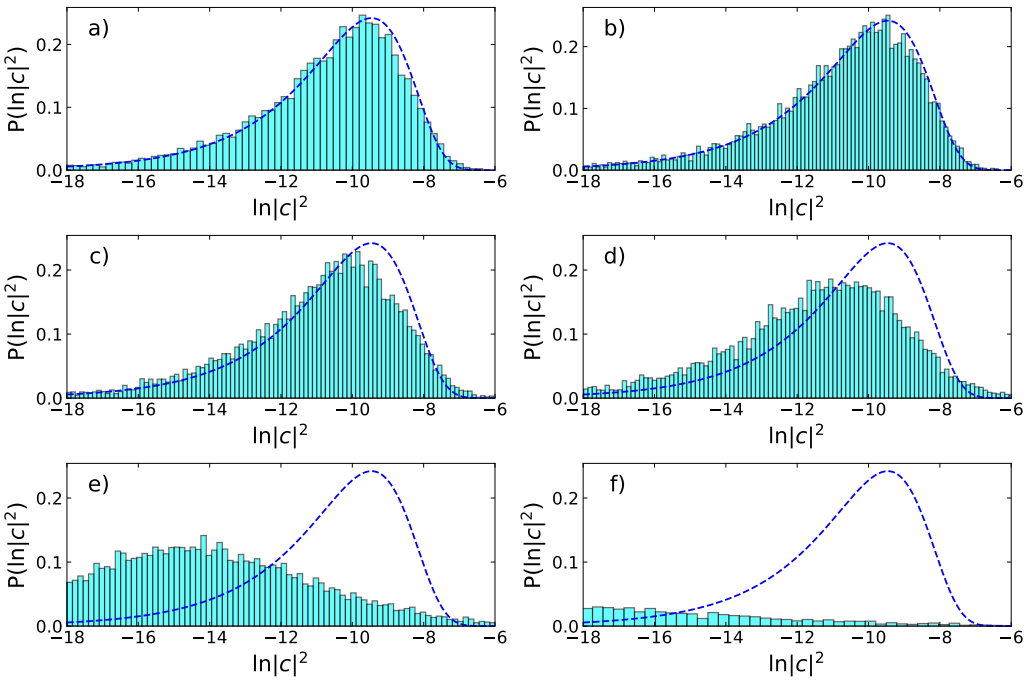

Figure 5.6: Porter-Thomas distribution for the inetracting Aubry-André model, for $L = 16$. The perturbation strength for each panel is a) $\lambda = 0.1$, b) $\lambda = 0.5$, c) $\lambda = 0.8$, d) $\lambda = 1.1$, e) $\lambda = 1.4$ and f) $\lambda = 2.0$. The blue dashed line correspond to the Porter-Thomas distribution Eq. (2.18).

Panels a) and b) correspond to $\lambda = 0.1$ and 0.5 respectively. According to the $\langle\tilde{r}\rangle$ analysis the system is chaotic, therefore the states at the middle of the spectrum should be extended and behave as random vectors, the information given by the analysis of the weights are in agreement whit this, since it is clear that there is an excellent correspondence between the histogram and the Porter-Thomas distribution. Panel c) and d) corresponds to $\lambda = 0.8$ and 1.1, according to the $\langle\tilde{r}\rangle$ analysis, the system is chaotic when $\lambda = 0.8$ however

it has been showed through the $\frac{IPR_n}{IPR_{GOE}}$ analysis that the systems is not chaotic and the graph c) confirms this statement since there is not correspondence between the Porter-Thomas distribution and the histogram, even when the state is located at the middle of the spectrum; on the other hand, as it was expected for the amplitude $\lambda = 1.1$, there is not correspondence between the Porter-Thomas distribution and the histogram. Panel e) and f) correspondence to the amplitudes $\lambda = 1.4$ and 2.0 respectively, it was expected a lack of correspondence between histograms and the Porter-Thomas distribution since these amplitudes belong to the extend zone.

5.6 Adiabatic gauge potential

In this section we study the transition from the integrable regime to the chaotic regime using the AGP. Since we are interesting in the integrability breaking we still consider the anisotropy as the generator of deformations, then $\gamma = \Delta$.

The Hamiltonian is given by

$$H_{AA}(\gamma) = \sum_{k=1}^{L-1}(S_k^x S_{k+1}^x + S_k^y S_{k+1}^y + \gamma S_k^z S_{k+1}^z) + \sum_{k=1}^{L}\lambda_k S_k^z. \tag{5.3}$$

Let be $|\psi_n(\gamma)\rangle$ a base eigenstate of the Hamiltonian $H_{AA}(\gamma)$ so $H_{AA}(\gamma)|\psi_n(\gamma)\rangle = E_n(\gamma)|\psi_n(\gamma)\rangle$. On the other hand,

$$\frac{\partial H_{AA}(\gamma)}{\partial \gamma} = \sum_{i=1}^{L-1} S_{k+1}^z S_k^z. \tag{5.4}$$

Following the procedure analogous to the Sec. 4.6.1, we can express the AGP as

$$||\mathscr{A}_\gamma||^2 = \frac{1}{\mathscr{D}}\sum_n \sum_{m\neq n} \frac{\omega_{mn}^2}{(\omega_{mn}^2+\mu^2)^2} |\sum_l \sum_k C_{nl}^* C_{nk} \langle\psi_l| \sum_{i=1}^{L-1} S_{k+1}^z S_k^z |\psi_k\rangle|^2. \tag{5.5}$$

Where $|\psi_k\rangle$ is a base eigenstate of $\partial_\gamma H_{AA}(\gamma)$.

We already know that the model XXZ without perturbation is integrable for the anisotropy value $\Delta = 0.48$. We found we found in Sec. 4.6 that the rescaled AGP norm $||\mathscr{A}||^2/L$ follows the polynomial behavior given by $||\mathscr{A}||^2/L = 0.04064L - 0.25349$. The next step is to analyze what happens when the Harper potential is turned on. In order to study this transition we increase the Harper potential amplitude.

The figure 5.7 shows the AGP norm rescaled, we present the results in semi-log scale. We vary the amplitude of λ, we choose seven different amplitudes (see the chart legend). The red solid line is the curve $||\mathscr{A}||^2/L = 0.04064L - 0.25349$ for the integrable case.

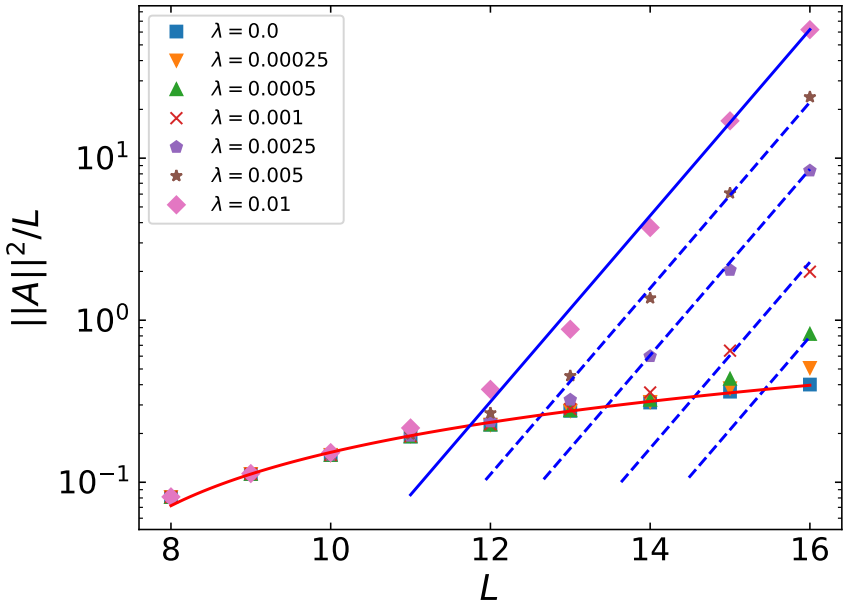

Figure 5.7: Rescaled AGP norm $||\mathscr{A}||^2/L$ for the Aubry-André model with $\Delta = 0.48$. The red solid line is an adjust of a first order polynomial given by $||\mathscr{A}||^2/L = 0.04064L - 0.25349$. The blue solid line is the exponential fitting $||\mathscr{A}||^2/L \propto e^{-1.32L}$

The blue solid line is the exponential fitting $||\mathscr{A}||^2/L \propto e^{-1.32L}$. It is interesting that for the smallest system the behavior is the same, however as we increase the system size the AGP norm behavior changes. This change depends on the Harper potential amplitude, since for the smallest amplitudes the change occurs for large systems, however as the Harper potential amplitude increases the change occurs for smaller systems. With this analysis it is possible to claim that the amplitude needed to break the integrability of the system depends on system size, therefore the next task is to find the crossover points between the blue lines and the red line.

Figure 5.8 depicts the scaling of the Harper potential amplitude λ, we present it in semi-log scale. The blue squares are the crossover points between the integrable behavior and the chaotic behavior shown in Fig. 5.7. The red solid line is the fitting to the data given by $\lambda = 123.31e^{-0.8}$. This is the main result of our work since with the study of the AGP we could give a relation between the amplitude needed to break the integrability of the system and the system size. For instance, for $L = 16$ the amplitude needed to break the integrability of the system according to AGP prediction, it is $\lambda = 0.0003$; however, according

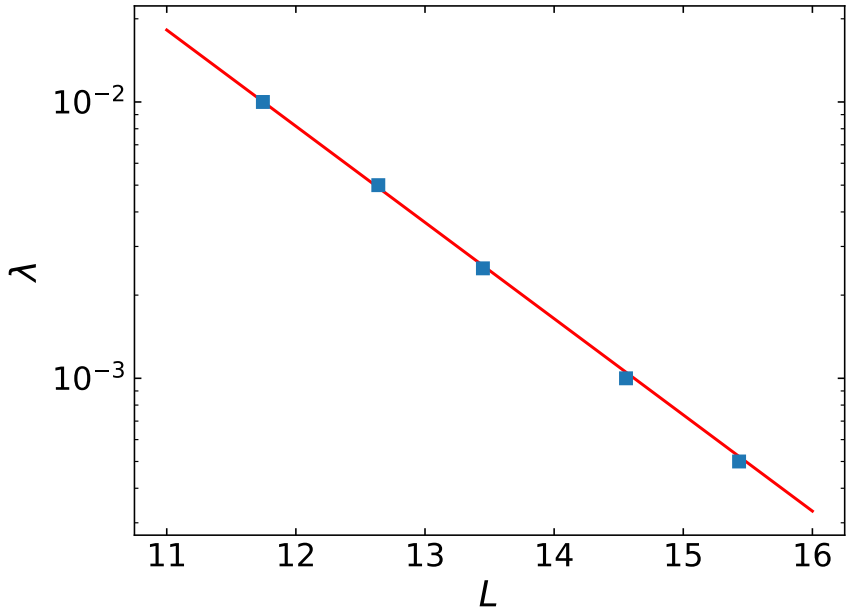

Figure 5.8: Harper potential amplitude for the interacting Aubry-André model λ. Blue squares are the crossover points between the red solid line and blues lines in Fig. 5.7. The red solid line is the fitting given by $\lambda = 123.31e^{-0.8L}$.

to the $\langle\tilde{r}\rangle$ prediction the system is not chaotic even for $\lambda = 0.1$, which is the advantage of the AGP analysis over standard RMT tools to detect the onset of chaos.

In this Chapter we studied the interacting Aubry-André model using different standard methods from RMT. First we use the ratio between consecutive spacings $\langle\tilde{r}\rangle$ to have a more clearly perspective of the general behavior of the interacting Aubry-André model. This quantity help us to choose six different amplitudes of λ and analyze them with tools from RMT. We choose the amplitudes in the three different regimes of the system, namely, chaotic, intermediate and localized regimes..

The information given by the level spacing distribution is in agreement with the results obtained by $\langle\tilde{r}\rangle$, when the perturbation $\lambda < 0.8$ the system is in a chaotic regime, the level spacing distribution shows an excellent agreement between the histograms and the Wigner-Dyson distribution, this means that the eigenenergies are correlated or there exist repulsion between them. For $0.8 < \lambda < 2.0$ the system is in an intermediate regime, there is a clear deviation between the histograms and the Wigner-Dyson distribution or the Poisson distribution. Finally, for $\lambda > 2.0$ the system is in a localized regime, this phenomena is

known as many-body localization which is considered a version os the well known Anderson localization but for interacting systems.

The study of the IPR provides more information about the system, in particular when the system is in the localized regime more of the states are localized, this is a signature of MBL phase. When the system is in the chaotic regime, the states at the middle of the spectrum are extended.The agreement between the distribution of energy eigenstates components and the Porter-Thomas distribution means that the energy eigenstates in the chaotic regime behave as uncorrelated random vector with a Gaussian distribution.

The AGP shows a remarkable sensitive to detect chaos and we obtain a relation between the system size and the amplitude λ to predict the onset of chaos. For instance, the prediction given by the AGP for a system with $L = 16$ spins is $\lambda = 0.0003$, however the $\langle \tilde{r} \rangle$ predicts that the systems in the chaotic regime for $\lambda = 0.2$.

Chapter 6

Conclusions and perspectives

We implemented numerically the XXZ model with and without perturbations, and the interacting Aubry-André model. We reached large enough system sizes to describe the statistical properties of the system. The mean ratio between consecutive spacings is a good tool to have a general perspective of the system behavior; for small system sizes, the finite sizes effects are present. The mean ratio between consecutive spacings detects the transition from the integrable regime to the chaotic regime. For the XXZ model with local perturbations, we found consistent results with the results published in the literature. For the interacting Aubry-André model, we found results consistent with experiments, this model present three different phases. However, the mean ratio between consecutive spacings is less sensitive than the AGP, in the case of the Aubry-André model, there are three orders of magnitude of difference.

The level spacing distribution has been historically the most used tool to detect chaos; however, it presents some disadvantages compared to other quantities, in our study the unfolding procedure was a problem since we study long-range correlations, then it has been shown that just global unfolding preserve long-range correlations, so we discarded the local unfolding. Another problem is that an extra analysis is required if our proposal is to study the onset of chaos, for example in the paper [20] the indicator β is used to measure deviations between the histogram and the Wigner-Dyson distribution. There are systems that do not present correlations between eigenenergies such as the Aubry-André model without interactions.

The level number variance presents similar problems to the level spacing distribution, however it gives us valuable information about the correlations between energy levels,

since we perform a statistical study we needed to use large system sizes to avoid possible finite sizes effects.

On the other hand, the study of eigenstates structure and statistics gives us valuable information. The IPR is one of the more appropriated quantities, since it could give us information about the delocalization and typically appears in the studies of dynamics, for example through the survival probability. For the XXZ model with local perturbations we found that when there is not perturbation the IPR presents strong fluctuations, however when the perturbation is large enough to break the integrability of the system, the IPR of the states at the center of the spectrum is quite similar and close to the limit of extended states a clear signature of chaos. For the interacting Aubry-André two different regions appear: the intermediate region where there are many localized states but also many extended states; and the localized zone, where most of the states are localized.

The Porter-Thomas distribution is an excellent tool to identify if an eigenstate is chaotic or not, however this statistic is just for random states. For the XXZ model we found consistent results with the prediction given by the mean ratio between consecutive spacings. For the interacting Aubry-André model we found that the ration between consecutive spacing fails since close to the intermediate regime we found deviations between the Porter-Thomas distribution and the histogram, which means that not all states are in this regime.

We reproduced results published in the work [15]. Finally, the AGP shows a remarkable sensitive to detect chaos. The AGP may work in the total Hilbert space and it is not needed to avoid most symmetries as is possible, since the AGP measure deformations of eigenstates and no correlations between eigenenergies. We found that the impurities at the edges of the chain could change the behavior of the AGP, there are amplitudes of the impurity at the edges where the AGP presents an exponential behavior, a more detailed analysis is required to know why the AGP presents this transition. Another question that emerges, is if the interval predicted in [15] $[0.69, 1.38]$ correct?

The main result of our study of the AGP is that we could give a relation between the amplitude needed to break the integrability of the system and the system size. We found two different relations for the XXZ model with local perturbations and the Aubry-André model. For the Aubry-André model we found that AGP predicts the onset of chaos earlier than the $\langle \tilde{r} \rangle$ is three magnitude orders.

Another big question is why completely localized states appear in the middle of

the spectrum and why they only appear for large system sizes. One of the biggest question is, what is the behavior of the AGP for ensembles of random matrix theory since there are not studies yet.

Another important problem is to analyze the behavior of the AGP around the transition from an intermediate phase to a localized one in the interacting Aubry-André model. We leave this analysis for future work.

Appendix A

XXZ model with an impurity at the beginning of the chian

Here we present the results obtained for the XXZ model with an impurity at the beginning of the chain, the Hamiltonian is given by

$$H_{\epsilon_1} = \sum_{k=1}^{L-1} (S_k^x S_{k+1}^x + S_k^y S_{k+1}^y + \Delta S_k^z S_{k+1}^z) + \epsilon_1 S_1^z. \tag{A.1}$$

We are interested on the behavior of the AGP but now adding an impurity in one edge. Following the analysis done in the previous sections, we take the anisotropy as the generator of deformations, then we turn on the impurity and increase its amplitude.

Figure A.1 shows the behavior of the rescaled AGP norm as function of the system size. The red solid line is a polynomial fitting given by $||\mathscr{A}||^2/L = 0.04064L - 0.25349$, this fitting corresponds to the data for $\epsilon_1 = 0$, namely the system is integrable. The blue solid line is an exponential fitting given by $||\mathscr{A}||^2/L = 0.0003e^{0.55L}$. It is interesting that the AGP presents two different behaviors, we expect that the AGP fluctuates around the red solid line, however after a some value of the amplitude the AGP changes its behavior from the polynomial to the exponential. Something important to note is that the exponent is less than predicted for chaotic systems, namely the exponent found is $\kappa = 0.55$ and the lower limit for chaotic systems according to [15] is $\kappa = log(2) \approx 0.7$. A more detailed analysis is required to know why the AGP presents this change of behavior. However, this analysis is outside the scope of this work.

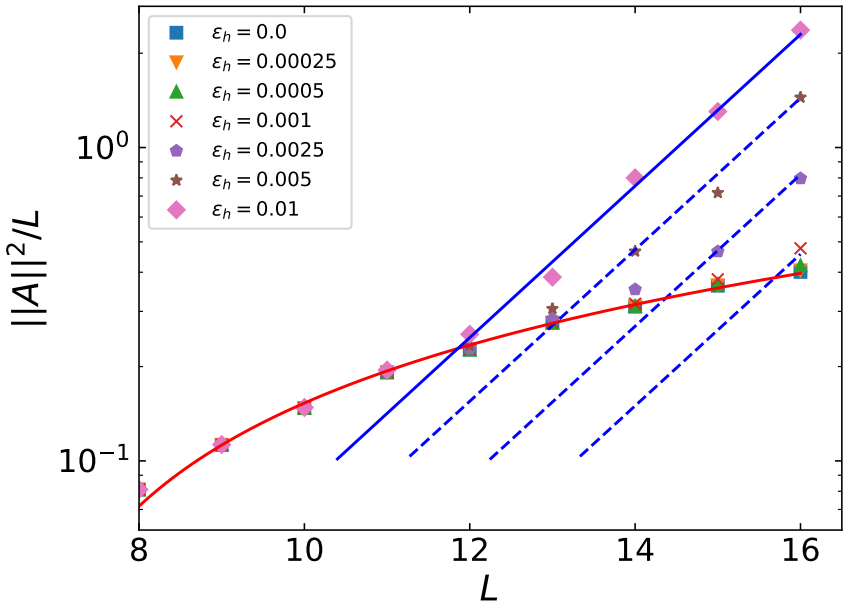

Figure A.1: Rescaled AGP norm $||\mathscr{A}||^2/L$ for the XXZ model with one impurity at the beginning of the chain with $\Delta = 0.48$. The blue solid line is an exponential fitting given by $||\mathscr{A}||^2/L = 0.0003e^{0.55L}$. The red solid line is the an fitting of a first order polynomial given by $||\mathscr{A}||^2/L = 0.04064L - 0.25349$.

Bibliography

[1] F. Borgonovi et al. "Quantum chaos and thermalization in isolated systems of interacting particles". In: *Phys. Rep.* 626 (2016), pp. 1–58.

[2] L. D'Alessio et al. "From quantum chaos and eigenstate thermalization to statistical mechanics and thermodynamics". In: *Adv. Phys.* 65.3 (2016), pp. 239–362.

[3] D. L. Shepelyansky. "Quantum chaos and quantum computers". In: *Physica Scripta* 2001.T90 (Jan. 2001), p. 112. DOI: 10.1238/Physica.Topical.090a00112. URL: https://dx.doi.org/10.1238/Physica.Topical.090a00112.

[4] Simon-Dominik Börner et al. "Classical chaos in quantum computers". In: *Phys. Rev. Res.* 6 (3 Aug. 2024), p. 033128. DOI: 10.1103/PhysRevResearch.6.033128. URL: https://link.aps.org/doi/10.1103/PhysRevResearch.6.033128.

[5] D. Basilewitsch et al. *Chaotic fluctuations in a universal set of transmon qubit gates.* 2024. arXiv: 2311.14592 [quant-ph]. URL: https://arxiv.org/abs/2311.14592.

[6] J. Zhang et al. "Observation of a many-body dynamical phase transition with a 53-qubit quantum simulator". In: 551.7682 (Nov. 2017), pp. 601–604. DOI: 10.1038/nature24654. arXiv: 1708.01044 [quant-ph].

[7] I. Bloch, J. Dalibard, and W. Zwerger. "Many-body physics with ultracold gases". In: *Rev. Mod. Phys.* 80 (3 July 2008), pp. 885–964. DOI: 10.1103/RevModPhys.80.885. URL: https://link.aps.org/doi/10.1103/RevModPhys.80.885.

[8] Adway Kumar Das et al. *Proposal for many-body quantum chaos detection.* 2024. arXiv: 2401.01401 [cond-mat.stat-mech]. URL: https://arxiv.org/abs/2401.01401.

[9] Juan Maldacena, Stephen H. Shenker, and Douglas Stanford. "A bound on chaos". In: *Journal of High Energy Physics* 2016.8, 106 (Aug. 2016), p. 106. DOI: 10.1007/JHEP08(2016)106. arXiv: 1503.01409 [hep-th].

[10] Eugene P. Wigner. "On the Distribution of the Roots of Certain Symmetric Matrices". In: *Ann. Math.* 67.2 (1958), pp. 325–327. ISSN: 0003486X, 19398980. URL: http://www.jstor.org/stable/1970008 (visited on 10/17/2024).

[11] Freeman J. Dyson. "The threefold way. Algebraic structure of symmetry groups and ensembles in quantum mechanics". In: *J. Math. Phys.* 3.6 (1962), pp. 1199–1215.

[12] O. Bohigas, M. J. Giannoni, and C. Schmit. "Characterization of Chaotic Quantum Spectra and Universality of Level Fluctuation Laws". In: *Phys. Rev. Lett.* 52 (1 Jan. 1984), pp. 1–4. DOI: 10.1103/PhysRevLett.52.1. URL: https://link.aps.org/doi/10.1103/PhysRevLett.52.1.

[13] M. L. Mehta. *Random matrices*. Elsevier, 2004.

[14] Michael V. Berry and Michael Tabor. "Level clustering in the regular spectrum". In: *Proc. R. Soc. A: Math. Phys. Eng. Sci.* 356 (1977), pp. 375–394. URL: https://api.semanticscholar.org/CorpusID:123407512.

[15] Mohit Pandey et al. "Adiabatic Eigenstate Deformations as a Sensitive Probe for Quantum Chaos". In: *Phys. Rev. X* 10 (4 Oct. 2020), p. 041017. DOI: 10.1103/PhysRevX.10.041017. URL: https://link.aps.org/doi/10.1103/PhysRevX.10.041017.

[16] M. Kolodrubetz et al. "Geometry and non-adiabatic response in quantum and classical systems". In: *Phys. Rep.* 697 (June 2017), pp. 1–87. ISSN: 0370-1573. DOI: 10.1016/j.physrep.2017.07.001. URL: http://dx.doi.org/10.1016/j.physrep.2017.07.001.

[17] Don N. Page. "Geometrical description of Berry's phase". In: *Phys. Rev. A* 36 (7 Oct. 1987), pp. 3479–3481. DOI: 10.1103/PhysRevA.36.3479. URL: https://link.aps.org/doi/10.1103/PhysRevA.36.3479.

[18] P. Orlov et al. "Adiabatic eigenstate deformations and weak integrability breaking of Heisenberg chain". In: *Phys. Rev. B* 107.18 (2023), p. 184312.

[19] B. Pozsgay et al. "Adiabatic gauge potential and integrability breaking with free fermions". In: *SciPost Phys.* 17.3 (Sept. 2024). ISSN: 2542-4653. DOI: 10.21468/scipostphys.17.3.075. URL: http://dx.doi.org/10.21468/SciPostPhys.17.3.075.

[20] E. J. Torres-Herrera and Lea F. Santos. "Local quenches with global effects in interacting quantum systems". In: *Phys. Rev. E* 89 (6 June 2014), p. 062110. DOI: 10.1103/PhysRevE.89.062110. URL: https://link.aps.org/doi/10.1103/PhysRevE.89.062110.

[21] Lea F. Santos, Francisco Pérez-Bernal, and E. Jonathan Torres-Herrera. "Speck of chaos". In: *Phys. Rev. Res.* 2 (4 Oct. 2020), p. 043034. DOI: 10.1103/PhysRevResearch.2.043034. URL: https://link.aps.org/doi/10.1103/PhysRevResearch.2.043034.

[22] J. A. Méndez-Bermúdez et al. "Understanding quantum scattering properties in terms of purely classical dynamics: Two-dimensional open chaotic billiards". In: *Phys. Rev. E* 66 (4 Oct. 2002), p. 046207. DOI: 10.1103/PhysRevE.66.046207. URL: https://link.aps.org/doi/10.1103/PhysRevE.66.046207.

[23] T. Guhr, A. Müller-Groeling, and H. A. Weidenmüller. "Random-matrix theories in quantum physics: common concepts". In: *Physics Reports* 299.4–6 (June 1998), pp. 189–425. ISSN: 0370-1573. DOI: 10.1016/s0370-1573(97)00088-4. URL: http://dx.doi.org/10.1016/S0370-1573(97)00088-4.

[24] F. M. Izrailev. "Simple models of quantum chaos: Spectrum and eigenfunctions". In: *Phys. Rep.* 196.5 (1990), pp. 299–392. ISSN: 0370-1573. DOI: https://doi.org/10.1016/0370-1573(90)90067-C. URL: https://www.sciencedirect.com/science/article/pii/037015739090067C.

[25] V. Oganesyan and D. A. Huse. "Localization of interacting fermions at high temperature". In: *Phys. Rev. B* 75 (15 Apr. 2007), p. 155111. DOI: 10.1103/PhysRevB.75.155111. URL: https://link.aps.org/doi/10.1103/PhysRevB.75.155111.

[26] Y. Y. Atas et al. "Distribution of the Ratio of Consecutive Level Spacings in Random Matrix Ensembles". In: *Phys. Rev. Lett.* 110 (8 Feb. 2013), p. 084101. DOI: 10.1103/PhysRevLett.110.084101. URL: https://link.aps.org/doi/10.1103/PhysRevLett.110.084101.

[27] C. L. Bertrand and A. M. García-García. "Anomalous Thouless energy and critical statistics on the metallic side of the many-body localization transition". In: *Phys. Rev. B* 94 (14 Oct. 2016), p. 144201. DOI: 10.1103/PhysRevB.94.144201. URL: https://link.aps.org/doi/10.1103/PhysRevB.94.144201.

[28] A. Pandey and R. Ramaswamy. "Level spacings for harmonic-oscillator systems". In: *Phys. Rev. A* 43 (8 Apr. 1991), pp. 4237–4243. DOI: 10.1103/PhysRevA.43.4237. URL: https://link.aps.org/doi/10.1103/PhysRevA.43.4237.

[29] Pablo R. Zangara et al. "Time fluctuations in isolated quantum systems of interacting particles". In: *Phys. Rev. E* 88 (3 Sept. 2013), p. 032913. DOI: 10.1103/PhysRevE.88.032913. URL: https://link.aps.org/doi/10.1103/PhysRevE.88.032913.

[30] Tómas A. Brody et al. "Random-matrix physics: spectrum and strength fluctuations". In: *Rev. Mod. Phys.* 53.3 (1981), p. 385.

[31] Li H. Sun L. Z. Nie Q. "Randomness of Eigenstates of Many-Body Quantum Systems". In: *Entropy (Basel)* (2019). DOI: 10.3390/e21030227.

[32] P. W. Anderson. "Absence of Diffusion in Certain Random Lattices". In: *Phys. Rev.* 109 (5 Mar. 1958), pp. 1492–1505. DOI: 10.1103/PhysRev.109.1492. URL: https://link.aps.org/doi/10.1103/PhysRev.109.1492.

[33] G. Casati et al. "Quantum ergodicity and localization in conservative systems: The Wigner band random matrix model". In: *Physics Letters A* 223.6 (1996), pp. 430–435.

[34] B. V. Chirikov. "An example of chaotic eigenstates in a complex atom". In: *Phys. Lett. A.* 108.2 (1985), pp. 68–70.

[35] Y. Liu et al. "Quantum algorithms for inverse participation ratio estimation in multi-qubit and multiqudit systems". In: *Physical Review A* 111.5 (May 2025). ISSN: 2469-9934. DOI: 10.1103/physreva.111.052614. URL: http://dx.doi.org/10.1103/PhysRevA.111.052614.

[36] N. Ullah and Ch. E. Porter. "INVARIANCE HYPOTHESIS AND HAMILTONIAN MATRIX ELEMENT CORRELATIONS". In: *Phys. Letters* Vol: 6 (Sept. 1963). DOI: 10.1016/0031-9163(63)90484-0. URL: https://www.osti.gov/biblio/4683449.

[37] E. J. Torres-Herrera and Lea F. Santos. "Extended nonergodic states in disordered many-body quantum systems". In: *Ann. Phys. (Berlin)* 529.7 (Jan. 2017). ISSN: 1521-3889. DOI: 10.1002/andp.201600284. URL: http://dx.doi.org/10.1002/andp.201600284.

[38] Charles E. Porter and Robert G. Thomas. "Fluctuations of nuclear reaction widths". In: *Phys. Rev.* 104.2 (1956), p. 483.

[39] E. J. Torres-Herrera, Manan Vyas, and Lea F. Santos. "General features of the relaxation dynamics of interacting quantum systems". In: *New J. Phys.* 16.6 (2014), p. 063010.

[40] E. Lieb, T. Schultz, and D. Mattis. "Two soluble models of an antiferromagnetic chain". In: *Ann. Phys.* 16.3 (1961), pp. 407–466.

[41] Antonio Sergio Teixeira Pires. "The Heisenberg model". In: *Theoretical Tools for Spin Models in Magnetic Systems*. 2053-2563. IOP Publishing, 2021, 1-1 to 1–16. ISBN: 978-0-7503-3879-0. DOI: 10.1088/978-0-7503-3879-0ch1. URL: https://dx.doi.org/10.1088/978-0-7503-3879-0ch1.

[42] A. N. Kirillov and N. Yu Reshetikhin. "Exact solution of the integrable XXZ Heisenberg model with arbitrary spin. I. The ground state and the excitation spectrum". In: *J. Phys. A* 20 (1987), pp. 1565–1585. DOI: 10.1088/0305-4470/20/6/038.

[43] A. Polkovnikov et al. "Colloquium: Nonequilibrium dynamics of closed interacting quantum systems". In: *Rev. Mod. Phys.* 83 (3 Aug. 2011), pp. 863–883. DOI: 10.1103/RevModPhys.83.863. URL: https://link.aps.org/doi/10.1103/RevModPhys.83.863.

[44] T. Fukuhara et al. "Quantum dynamics of a mobile spin impurity". In: *Nature Physics* 9.4 (Feb. 2013), pp. 235–241. ISSN: 1745-2481. DOI: 10.1038/nphys2561. URL: http://dx.doi.org/10.1038/nphys2561.

[45] L F Santos. "Integrability of a disordered Heisenberg spin-1/2 chain". In: *J. Phys. A Math. Gen.* 37.17 (Apr. 2004), pp. 4723–4729. ISSN: 1361-6447. DOI: 10.1088/0305-4470/37/17/004. URL: http://dx.doi.org/10.1088/0305-4470/37/17/004.

[46] P. G. Harper. "Single band motion of conduction electrons in a uniform magnetic field". In: *Proc. Phys. Soc. Section A* 68.10 (1955), p. 874.

[47] S. Y. Jitomirskaya. "Metal-insulator transition for the almost Mathieu operator". In: *Ann. Math.* (1999), pp. 1159–1175.

[48] S. Aubry and G. André. "Analyticity breaking and Anderson localization in incommensurate lattices". In: *Ann. Israel Phys. Soc* 3.133 (1980), p. 18.

[49] H. Li, Y. Wang, and et. al. "Observation of critical phase transition in a generalized Aubry-André-Harper model with superconducting circuits". In: *npj Quantum Information* 9.1 (Apr. 2023). ISSN: 2056-6387. DOI: 10.1038/s41534-023-00712-w. URL: http://dx.doi.org/10.1038/s41534-023-00712-w.

[50] Shenglong Xu et al. "Butterfly effect in interacting Aubry-André model: Thermalization, slow scrambling, and many-body localization". In: *Physical Review Research* 1.3 (2019), p. 032039.

[51] M. Schreiber et al. "Observation of many-body localization of interacting fermions in a quasirandom optical lattice". In: *Science* 349.6250 (Aug. 2015), pp. 842–845. ISSN: 1095-9203. DOI: 10.1126/science.aaa7432. URL: http://dx.doi.org/10.1126/science.aaa7432.

[52] H. Q. Lin. "Exact diagonalization of quantum-spin models". In: *Phys. Rev. B* 42.10 (1990), p. 6561.

[53] Alexander Weiße and Holger Fehske. "Exact Diagonalization Techniques". In: *Computational Many-Particle Physics*. Berlin, Heidelberg: Springer Berlin Heidelberg, 2008, pp. 529–544. DOI: 10.1007/978-3-540-74686-7_18. URL: https://doi.org/10.1007/978-3-540-74686-7_18.

[54] Jung-Hoon Jung and Jae Dong Noh. "Guide to Exact diagonalization study of Quantum Thermalization". In: *J. Korean Phys. Soc.* 76 (2020), pp. 670–683.

[55] Alcaraz F. C et al. "Surface exponents of the quantum XXZ, Ashkin-Teller and Potts models". In: *Journal of Physics A: Mathematical and General* 20.18 (Dec. 1987), p. 6397. DOI: 10.1088/0305-4470/20/18/038. URL: https://doi.org/10.1088/0305-4470/20/18/038.

[56] C. Diaz-Mejia et al. "Persistent revivals in a system of trapped bosonic atoms". In: *Physics Letters A* 493 (2024), p. 129262. ISSN: 0375-9601. DOI: https://doi.org/10.1016/j.physleta.2023.129262. URL: https://www.sciencedirect.com/science/article/pii/S0375960123006424.

[57] A. Pizzi et al. “Genuine quantum scars in many-body spin systems”. In: *Nature Communications* 16.1 (July 2025). ISSN: 2041-1723. DOI: 10.1038/s41467-025-61765-3. URL: http://dx.doi.org/10.1038/s41467-025-61765-3.